UNIVERSITÉ DU QUÉBEC

MÉMOIRE PRÉSENTÉ À
L'UNIVERSITÉ DU QUÉBEC À TROIS-RIVIÈRES

COMME EXIGENCE PARTIELLE
DE LA MAÎTRISE EN GÉNIE ÉLECTRIQUE

PAR
ALVARO OMAR MACIAS FERNANDEZ

IDENTIFICATION EN LIGNE POUR LA GESTION D'ÉNERGIE DES SYSTÈMES MULTI-STACKS

SEPTEMBRE 2018

UNIVERSITY OF QUEBEC

THESIS SUBMITTED TO
UNIVERSITÉ DU QUÉBEC À TROIS-RIVIÈRES

IN PARTIAL FULFILLMENT OF THE REQUIREMENTS FOR THE DEGREE OF
MASTER IN ELECTRICAL ENGINEERING

BY
ALVARO OMAR MACIAS FERNANDEZ

ONLINE IDENTIFICATION FOR ENERGY MANAGEMENT OF MULTI-STACK SYSTEMS

SEPTEMBER 2018

UNIVERSITÉ DU QUÉBEC À TROIS-RIVIÈRES

MAÎTRISE EN GÉNIE ÉLECTRIQUE (M. SC. A.)

Programme offert par l'Université du Québec à Trois-Rivières

IDENTIFICATION EN LIGNE POUR LA GESTION D'ÉNERGIE DES SYSTÈMES MULTI-STACKS

PAR

ALVARO OMAR MACIAS FERNANDEZ

Loïc Boulon	Université du Québec à Trois-Rivières
Hicham Chaoui	Carleton University
João Trovão	Université de Sherbrooke
Mohamed Becherif	Université de Technologie de Belfort Montbéliard

Résumé

La dépendance aux combustibles fossiles et l'effet de serre peuvent être réduits par l'électrification du train de puissance des véhicules. Afin d'assurer une réelle diminution de la pollution, l'énergie électrique doit être générée par des sources vertes et renouvelables. De nos jours, les véhicules à batterie (BEV) montrent une acceptation du marché et sont à zéro émission locale, mais il a deux inconvénients principaux : un long temps de recharge et une autonomie limitée. La combinaison d'une pile à combustible en tant que source primaire et d'une source secondaire telle qu'une batterie ou un super-condensateur bénéficie d'atouts particuliers, tels qu'un rendement plus élevé que les moteurs à combustion interne, plus d'autonomie que les BEV et une maintenance aisée. Un système de pile à combustible à plusieurs stacks (MFCS) est un ensemble de piles à combustible indépendantes (PAC) de faibles puissances utilisé en lieu et place d'une PAC de forte puissance. Ainsi, les différentes modules peuvent fonctionner ensemble pour prolonger la durée de vie du système et augmenter les performances. Néanmoins, le Tableau 1-1 présente évaluation du coût du système de 25 kW à mono et multi PAC, ce qui montre que le coût initial d'un MFCS est plus élevé. La répartition de puissance entre les PACs doit être contrôlé par une stratégie de gestion de l'énergie. Les stratégies peuvent être catégorisées en deux grands groupes : basées sur des règles et basées sur l'optimisation. Le groupe à base de règles comprend des règles déterministes et logique floue, qui peuvent apparaître sous la forme d'approches conventionnelles, adaptatives et prédictives. Le groupe à base d'optimisation est composé d'une optimisation globale et en temps réel dans laquelle une fonction de coût est utilisée pour définir la consommation de combustible et l'efficacité du système. Cette thèse traite de

la conception d'une stratégie en ligne pour un MFCS dans une connexion parallèle, comme cela est montré dans la Figure 1.4, pour améliorer l'économie de combustible ainsi que la durée de vie des PAC. À cet égard, une stratégie à deux couches est proposée pour partager la puissance entre quatre PACs et une batterie. La première couche (locale à chaque PAC) est responsable de la détermination en tout temps de la puissance maximale réelle et de l'efficacité de chaque PAC, étant donné que la variation des conditions de fonctionnement et le vieillissement influencent sensiblement les performances des PAC. Cette couche est composée d'un modèle semi-empirique et d'un filtre de Kalman. Ces modèles contiennent des paramètres physiques significatifs, qui permettent à un expert d'analyser les résultats de manière pratique. Dans ce travail, un modèle électrochimique proposé par Amphlett et al. est utilisé. Ce modèle est pour un nombre de cellules connectées en série et suppose le même comportement pour toutes les cellules. Dans ce modèle, la tension de sortie de la pile PEM (V_{FC}) est perçu comme la somme du potentiel de cellule réversible (E_{Nernst}) et de trois chutes de tension, à savoir activation (V_{act}), ohmique (V_{ohmic}) et concentration (V_{con}).

Le filtre utilisé met à jour les paramètres du modèle pour compenser les dérives de performance des FC. Le modèle discuté présente huit paramètres à identifier, qui sont listés dans au Tableau 2-1, avec les plages de variation correspondantes. L'intégration du filtre de Kalman pour estimer les paramètres du modèle d'une PAC réelle est illustrée à la Figure 2.6. Le filtre de Kalman est considéré comme un estimateur optimal et il peut estimer les paramètres d'intérêt à partir d'observations imprécises et incertaines. La Figure 2.7 présente un profil de courant et la tension et la température de mesure d'une PEMFC Horizon de 500 kW avec un cycle de conduite UDDS d'échelle, qui représente la condition de conduite urbaine. Dans la Figure 2.7, le tracé c) indique la comparaison de la tension estimée par la

modélisation en ligne avec la tension mesurée de la PAC. Comme il est observé, le modèle en ligne proposé est capable d'estimer la tension avec une précision satisfaisante. La Figure 2.8 compare la courbe de polarisation obtenue et la courbe de puissance du modèle en ligne avec les courbes de la PAC réelle. Selon cette figure, le modèle peut prédire la puissance maximale et le comportement de polarisation de la PAC avec une précision acceptable.

La deuxième couche (gestion globale) est responsable de la répartition de la puissance entre les composants. Cette couche prend en compte deux entrées par PAC, la puissance et l'efficacité maximales déterminées en temps réel par la première couche, ainsi que l'état de charge de la batterie (SOC) et la puissance demandée par le train de puissance pour effectuer le partage de puissance. La stratégie proposée, appelée stratégie de machine d'état adaptative, est illustrée à la Figure 3.5. Il utilise les deux premières entrées pour trier les PAC par la puissance maximale et les autres entrées pour faire l'allocation de puissance. L'objectif principal de cette stratégie est de minimiser le nombre de PAC pour fournir l'énergie requise et utiliser les PAC de manière efficace. Pour ce faire, elle utilise chaque PAC du point d'efficacité maximum jusqu'à la puissance maximale, en commençant par le PAC avec les meilleures performances. Les résultats finaux de la stratégie suggérée sont comparés à deux méthodes de partage de puissance couramment utilisées, à savoir Daisy Chain et Equal Distribution. La validation de la performance de la stratégie proposée est réalisée sur un banc d'essai développé au moyen de la technique « hardware-in-the-loop » (HIL). L'émulateur HIL développé peut être considéré comme un émulateur HIL complet pour le véhicule Némo, qui est un véhicule de laboratoire. Les spécifications de ce véhicule sont énumérées dans le Tableau 2-1. Comme on peut le voir sur la figure 1.4, il est composé d'une PAC réel, qui est un PEMFC Horizon 500 W à cathode ouverte, trois émulateurs PEMFC, qui seront discutés

au Chapitre 2, un modèle mathématique de batterie et quatre convertisseurs de courant continu. Afin d'étudier la performance de la stratégie proposée, trois scénarios différents ont été conçus. Dans le premier scénario, un profil de puissance de rampe a été utilisé pour montrer clairement la différence entre la distribution de la puissance entre les sources par les trois stratégies. Le deuxième scénario traite de l'évaluation des performances des stratégies tout en utilisant un vrai profil de conduite du véhicule Némo. Enfin, le dernier scénario a été conçu en utilisant un très long profil de puissance aléatoire pour évaluer le taux de dégradation des PACs. Les résultats de la stratégie proposée indiquent une amélioration prometteuse de la performance globale du système et un accroissement de la durée de vie du système en réduisant le temps de fonctionnement du FC avec un taux de dégradation plus élevé comme le montre la Figure 3.15.

Abstract

This thesis deals with design of an online energy management strategy (EMS) for a multi-stack fuel cell system (MFCS) to enhance the fuel economy as well as the fuel cells (FCs) lifetime. In this respect, a two-layer strategy is proposed to share the power among four FCs and a battery pack. The first layer (local to each FC) is held solely responsible for constantly determining real maximum power and efficiency of each FC since the operating conditions variation and ageing noticeably influence FCs' performance. This layer is composed of a FC semi-empirical model and a Kalman filter. The utilized filter updates the FC model parameters to compensate for the FCs' performance drifts. The second layer (global management) is held accountable for splitting the power among components. This layer takes two inputs per each FC, updated maximum power and efficiency, as well as the battery state of charge (SOC) and power train demanded power into account to perform the power sharing. The proposed EMS, which is called adaptive state machine strategy, employs the first two inputs to sort the FCs out and the other inputs to do the power allocation. The ultimate results of the suggested strategy are compared with two commonly used power sharing methods, namely Daisy Chain and Equal Distribution. The results of the suggested EMS indicate promising improvement in the overall performance of the system. The performance validation of the proposed strategy is conducted on a developed test bench by means of hardware-in-the-loop (HIL) technique.

Acknowledgments

First, I would like to thank my director, Professor Loïc Boulon, for his constructive comments and valuable guidance over my different stages of research. I am grateful to him for all the support during my internship period and the Master degree. I also thank the Mitacs Globalink and UQTR Foundation for the financial support.

I want to thank my co-director, Professor Hicham Chaoui, for the constant inspiration and valuable pieces of advice. He provided me with the tools that I needed to choose the right direction.

I am grateful to Professors Daniel Massicotte, Sousso Kelouwani, and Nadia Yousfi, for their encouragement and practical advice. I also want to thank to all my colleagues at the Hydrogen Research Institute for the nice working environment and all the good times shared.

Thanks to my friends during my master studies at Trois-Rivières, for all the trips, and outdoor activities during the summer and winter. Thanks to all the Persian communities for the warm welcome and making me feel at home.

Special thanks to my friend Mohsen Kandi for his priceless contributions to make this work possible. I could not have imagined having a better friend and advisor for my Master study.

Last but not the least; I would like to thank my family: my parents Maria del Carmen and Lorenzo, my brother Guillermo, and Elena for all the support and never letting me down.

Contents

Résumé iv

Abstract viii

Acknowledgments ix

Contents x

List of Tables xii

List of Figures xiii

Chapitre 1 - Introduction 15

1.1 Motivation 15

1.2 Literature review 19

1.3 Objective 24

1.4 Methodology 26

1.5 Thesis outline 27

Chapitre 2 - Modeling and Online Identification of a Fuel Cell System 28

2.1 Introduction 28

2.2 Power train model 29

2.3 Battery and DC-DC converter models 31

2.4 PEMFC modeling 32

2.4.1 Semi-empirical model 34

2.4.2 Resistor measurement 37

2.4.3 Online parameter identification 39

2.4.4 Results and discussion 43

2.5 Emulator design 49

2.5.1 Dynamic modeling 51

2.5.2 Model calibration 56

2.5.3 Results and discussion 61

2.6 Synopsis 64

Chapitre 3 - Energy management strategy design 65

3.1 Introduction 65

3.2 Multi-stack fuel cell system configuration 66

3.3 Energy management strategy 69

3.4 Results and discussion 73

3.4.1 Scenario 1: 74

3.4.2 Scenario 2: 79

3.4.3 Scenario 3: 81

Chapitre 4 - Conclusion 85

References 86

List of Tables

Table 1-1 25 kW Material handling equipment PEM MFCS analysis per unit [13] 18

Table 2-1 The unknown parameters of the semi-empirical model 37

Table 2-2 Current levels and PEMFC stack temperature during resistor measurement 38

Table 2-3 Kalman filter customization for the identification problem 42

Table 2-4 Average value of the estimated parameters (activation and concertation) 47

Table 2-5 Targeted parameters for model calibration 55

Table 2-6 DE parameters for definition 61

Table 2-7 Targeted parameters for model calibration 63

Table 3-1 Initial conditions for performing the ramp profile test 75

Table 3-2 Hydrogen consumption for the studied strategies and percentage reduction of the proposed strategy 81

Table 3-3 Degradation rate 82

Table 3-4 Hydrogen consumption comparison for the 300-h test and percentage reduction of the proposed strategy 84

List of Figures

Figure 1.1 Schematic diagram of a FCV drivetrain system 16

Figure 1.2 Classification of energy management strategies 20

Figure 1.3 MFCS configuration along with the EMS demonstration 25

Figure 1.4 The full-scale HIL 27

Figure 2.1 Battery equivalent circuit 31

Figure 2.2 PEMFC model categories 32

Figure 2.3 Evolution range of the PEMFC internal resistor with respect to current (a) and temperature (b) [47] 39

Figure 2.4 Different ways of processing the measured data in identification process 40

Figure 2.5 Online PEMFC modeling procedure 41

Figure 2.6 The employed set up for testing the online modeling 44

Figure 2.7 The voltage estimation result. a) Applied current profile to the PEMFC system, b) Measured temperature, c) Comparison of measured and estimated voltage (MSE: 0.1475) 45

Figure 2.8 Polarization curve a) and Power curve b) for the experimental and estimated curves by mean of Kalman filter with a MSE of 3.44 (by using the extracted parameter at 200 s) 46

Figure 2.9 PEMFC internal resistor evolution 47

Figure 2.10 The fluctuation of the activation loss parameters 48

Figure 2.11 The variation of the concentration loss parameter 49

Figure 2.12 The PEMFC system emulator 52

Figure 2.13 DE parameter evolution process for two-dimensional cost function [65] 57

Figure 2.14 DE flowchart 59

Figure 2.15 Representation of crossover process for seven parameters [65] 60

Figure 2.16 Current profile for testing the emulator 62

Figure 2.17 Voltage and temperature prediction by the emulator for duty cycle of 34, voltage evolution a), and temperature evolution b) 62

Figure 2.18 Voltage and temperature prediction by the emulator for duty cycle of 100, voltage evolution a), and temperature evolution b) 63

Figure 3.1 Operating characteristics of a PEMFC system from maximum efficiency to maximum power 66

Figure 3.2 multiple FC stack system architectures 67

Figure 3.3 Different configurations in a MFCS with DC-DC converters 68

Figure 3.4 Parallel architecture of the utilized MFCS 69

Figure 3.5 MFCS EMS configuration 70

Figure 3.6 Adaptive state machine EMS 72

Figure 3.7 Ramp profile 75

Figure 3.8 Power split for Condition 1, a) Equal distribution, b) Daisy Chain, and c) Adaptive State Machine 77

Figure 3.9 Power split for Condition 2, a) Equal distribution, b) Daisy Chain, c) Adaptive State Machine 78

Figure 3.10 Hydrogen consumption for the two conditions using the ramp profile 79

Figure 3.11 HWFET profile, a) Speed profile, b) Requested power from Nemo drive train 79

Figure 3.12 Power split for the three strategies, a) Equal distribution, b) Daisy Chain, and c) Adaptive State Machine 80

Figure 3.13 Random step power profile unit 81

Figure 3.14 Maximum power evolution during the 300-h test. a) Equal distribution, b) Daisy Chain, c) Adaptive State Machine 83

Figure 3.15 Operation time of each PEMFC during the 300-h test 83

Figure 3.16 Battery SOC evolution during the 300-h test. 84

Chapitre 1 - Introduction

1.1 Motivation

Anthropogenic emission of carbon dioxide has been declared as one of the leading causes of global warming around the world. In this regard, transportation sector is recognized as a primary contributor of emitting a noticeable amount of this greenhouse gas to the atmosphere mainly due to the combustion of fossil fuels such as gasoline in internal combustion engines (ICEs). Passenger cars are viewed as the principal source of transportation-related greenhouse gas discharge. Therefore, replacing the fossil fuel dependent energy sources by cleaner ones to power the vehicles can be stated as a vital step to defuse this global crisis.

Thanks to the technological advances in the electrification of vehicles' powertrains, several cleaner substitutes have been proposed for conventional vehicles. Hybrid electric vehicle (HEV) is one of the commercially available candidates, which is composed of a smaller ICE and an electric propulsion system. Although HEV generates less pollution than the conventional vehicle, it is still dependent on fossil fuels. Another potential substitute is pure battery electric vehicle (BEV), which is run on just batteries. BEV is a zero-emission vehicle. However, it suffers from two main disadvantages of long recharging time and limited driving range. The discussed drawbacks of the available options have created the basis for the advent of fuel cell system technology in the vehicular applications.

Among various types of fuel cells, proton exchange membrane fuel cell (PEMFC) has interesting characteristics, like low-temperature operation, high power density, and solid electrolyte to be utilized in a fuel cell vehicle (FCV) [1]. FCVs do not possess the restrictions of their rivals and benefit from particular assets, such as higher efficiency than lCEs, more autonomy than BEVs, easy maintenance, and being eco-friendly, by comparison [2]. FCVs powertrain is composed of a PEMFC as the primary power source, and a secondary source such as battery pack or/and supercapacitor, as shown in Figure 1.1. FCVs are experiencing a steady growth in the automotive market and several car companies have started introducing their products such as Honda FCX Clarity (2007), Mercedes-Benz F-Cell (2010), Hyundai Tucson FCEV (2014), Toyota Mirai (2015), Riversimple Rasa (2016), and Honda Clarity Fuel Cell (2016).

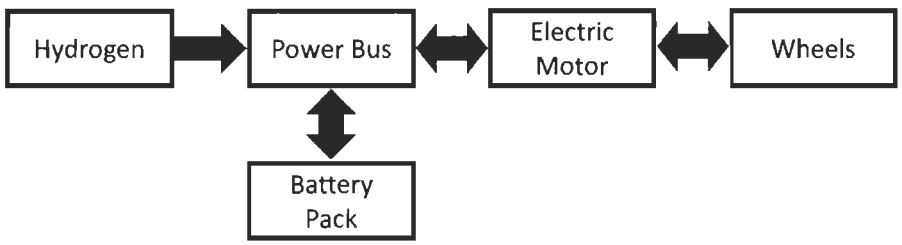

Figure 1.1 Schematic diagram of a FCV drivetrain system

However, some challenges have been posed to the development of this technology and FCVs need to rise to these challenges to be able to penetrate into the automotive market [3]. Some of these challenges are related to the renewable hydrogen production with comparable cost to fossil fuels, advances in material-based hydrogen storage, and providing the necessary infrastructures such as hydrogen stations, which are all in progress parallel to one another. Apart from the stated ongoing purposes, FCVs need to attract public attentions by offering a feasible substitute for conventional vehicles, particularly in terms of performance, reliability,

durability, and cost, to succeed in this super-competitive market. The existing cost projections of FCVs are mainly based on the presumption of large series production, usually 500,000 units / year. Therefore, in addition to performance and reliability, reaching the economy of scale can be considered highly important in the success of this technology in the confronted competition. The concept of using multi-stack fuel cell system (MFCS), which has been put forward recently [4], can be considered as a potential solution for the mentioned challenges regarding performance, reliability, and cost. A MFCS is an arrangement of low-power independent FCs, rather than one high-power FC, which can work together [5]. MFCSs can be configured in a way to lead to several economical and technical merits. In terms of performance, a MFCS can bring about high level of efficiency for the whole system. It is mainly due to the fact that a single fuel cell system has just one optimal operating point as opposed to a MFCS which has several optimal points. Regarding the reliability, the modular configuration in a MFCS, i.e. one converter per FC allowing independent control, provides a degraded mode of operation which is not accessible in single stack systems. This modularity makes the PEMFC system fault tolerance and enables the system to keep operating in case of a FC malfunction. Concerning the cost, it can be stated that employing a MFCS can help reaching the economy of scale and large-scale production numbers in the intended source of power. In fact, in a MFCS, the same module of PEMFC, which is produce in one production line, can be used for a wide range application in terms of the rated power because just the number of modules can be increased or decreased to meet the demand. On the other hand, the initial cost development of a MFCS is higher than a single stack system [6]. However, this drawback can be compensated by the discussed scale economy of modular configuration [7, 8]. The use of another source of energy, such as a battery pack, supercapacitor etc., besides a FC seems to be vital in vehicular applications due to the fact

that FCs have slow dynamics and are not capable of storing energy. The extra source reduces degradation rate of the FC by absorbing the power peaks and is also used for energy recovery. Common structures for hybridization of FCVs are FC-battery, FC-SC, and FC-battery-SC. All of these structures have their own advantages and disadvantages [9]. However, among them, FC-battery structure has been widely employed in practical FCVs [10, 11]. Among the existing rechargeable batteries, Li-ion battery is considered as a potential secondary source in FCVs since it has the merits of high capacity, several charge–discharge cycles and acceptable cost [12]. A cost breakdown of single and multi-fuel cell system of 25 kW is presented in Table 1-1. In this comparison, the same battery and hydrogen tank have been used in order to preserve the same energy capacity and compare capital costs, though the two systems could present different performances.

Table 1-1 25 kW Material handling equipment PEM MFCS analysis per unit [13]

Component	Single FC	MFCS
Battery	$ 10,000	$ 10,000
Hydrogen tank	$ 3,373	$ 3,373
DC/DC converter	$ 6,024	$ 4,990
Auxiliaries	$ 7,717	$ 15,968
Labor cost	$ 2,271	$ 3,527
Fuel cell	$ 6,972	$ 8,740
Total	$ 36,357	$ 46,598

With all the promising features of a MFCS and hybridization of sources, the performance of a FCV is influenced by a number of factors mainly due to the several sources with various

features. In this respect, the operating points of different components need to be determined efficiently by an energy management strategy (EMS) to increase the overall performance of the system. Indeed, this is the design of a suitable EMS which makes most of the above-mentioned advantages of MESs, such as reliability, durability, degraded mode operation, and even cost decline, feasible. The flexible structure of the MFCSs provide the powertrain with more degrees of freedom in terms of designing an EMS though the system becomes more complex to control.

1.2 Literature review

The overall performance of a FCV in terms of fuel or energy consumption significantly depends on the efficient coordination of powertrain component. Traditionally, an EMS attempts to optimize the fuel consumption of the system, without sacrificing the driving performance of the vehicle. It manages this important task through controlling the power flow between the PEMFC, battery, and the drive train. A well-designed EMS should assure reaching the following terms:

- The demanded power is always met by the output power of the electric motor.
- The state of the energy is always maintained within an optimal range in the battery.
- The PEMFC system operates within its optimal operating region.

Several EMSs have been utilized for splitting the power in the previously-discussed structures in FCVs. The majority of EMSs deal with a single-stack FC system. However, these methods are applicable to a MFCS with slight modifications. The existent EMSs in the literature fall into two categories of rule-based and optimization-based [9, 14], as represented in Figure 1.2 .

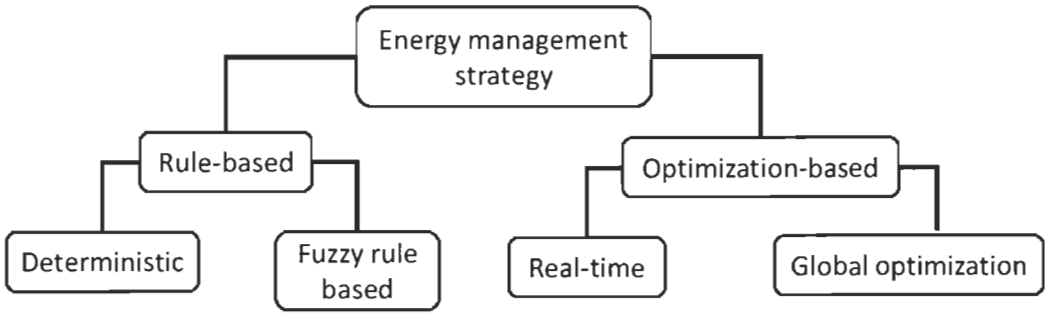

Figure 1.2 Classification of energy management strategies

The rule-based group comprises deterministic and fuzzy rule-based [15], which can appear in the form of conventional, adaptive, and predictive approaches. The optimization-based group is composed of global and real-time optimization in which a cost function is utilized to define fuel consumption and system efficiency. As mentioned earlier, there are a few works in the literature to touch on the subject of EMS design for MFCSs.

The following works fit into the first category of the presented EMSs. In [16] a simple rule-based EMS, composed of four FCs and a battery, is investigated in simulation. This control strategy considers 4 cases based on the SOC of the battery to adjust the requested energy from the FCs. In [4], a two-layer EMS is applied to a MFCS. The first layer is a state vector machine, which decides when to start or stop a FC based on the demanding power. The second layer sets the power level for the active FC by means of a rule-based algorithm. In [17], two simple rule-based algorithms are implemented in a MFCS with a parallel structure. The main purpose of the mentioned work is to demonstrate that parallel architecture can lead to a modular system in which the FC system is able to keep working even after losing one of the FCs. In [18], three power sharing algorithms, namely equal distribution, daisy chain, and optimal power splitting are compared. The comparison reveals that the optimal power splitting approach performs much better in high power region. In [17, 19], the

first two power sharing algorithms of the previous work are tested for a degraded mode operation scenario, where one of the FCs stops working. The influence of driving condition over the design of an EMS for a single fuel cell system has been considered in [20, 21], which is valid and expandable for multiple source systems. An optimized fuzzy logic controller (FLC) considering different traffic conditions is suggested in [21], and an adaptive FLC based on pattern recognition is proposed in [20]. These manuscripts indicate that the performance of a FCV is strikingly affected by the driving condition variations, and this is due to the fact that the fuel consumption is the direct result of the driving patterns formed by the traffic condition. Another type of rule-based EMS which has been successfully tested for multiple source systems is state machine based strategies [22-24]. This type of EMS can coordinate multiple units to meet the power demand while respecting the intrinsic characteristics of the sources. To do so, the power distribution is done with respect to the state change and the safe operating zones of the power sources. In brief, the rule-based strategies are simply implementable in real-time applications. However, they might result in the operation far from the optimal since the design is not based on the information of the whole trip. This weakness can be compensated by combining this methodology with other principles such as operating point tracking and optimization methods.

The second category of EMSs is based on optimization strategies which minimize a defined cost function by using global and real-time optimization techniques. Global optimization strategies usually have a priori knowledge of driving cycle, which can be translated to the demanded power from the FCV. These methods are usually applicable in the design of offline strategies, which can be utilized as a reference for evaluating new strategies. They also require a lot of time and cannot be used for real-time applications. In

[25], genetic algorithm is utilized to minimize the fuel consumption in a range extender vehicle by investigating several scenarios in terms of architecture and driving cycles. In [26], a multi objective optimization problem has been defined with the aim of minimizing the fuel consumption and vehicle cost by means of particle swarm optimization method. On the other hand, real-time optimization methods use an instantaneous cost function which only depends on the present data. In [27], a neural network modeling strategy is proposed to predict the behavior of a MFCS composed of four FCs. The application of this modeling technique is in the EMS design by means of model predictive control. There some other methods which use the optimal trajectory achieved by global optimization methods and try to devise a rule based method to improve this trajectory response for a wide range of conditions or cases. In [28], a multi-objective optimization method is proposed to ameliorate fuel economy as well as system durability. The proposed method is designed based on the results achieved by dynamic programming, and then the performance of the system is improved by altering the size of the battery. In [29], a combinatorial optimization approach is utilized to improve the decision making quality of the EMS off-line by a piecewise linearization of the supercapacitor power losses curve. In [30], a real time optimization strategy is implemented to reduce the hydrogen consumption, by searching the global maximum point in a virtual environment. Convex programming formulation, which benefits from a fast computational time, is proposed, in [10], to optimize the EMS as well as the main component sizes. In [31], a real time linear optimization is proposed for a MFCS, to find the optimal subset of FC to reach a constant demand during a specific time. This method estimates the remaining useful life to deduce the evolution of maximum and nominal power of each FC. To sum up, the global optimality can be reached by having the trip information in advance. Other cases may

lead to real-time optimality by defining an instantaneous cost function and introducing the necessary limitations to ensure self-sustainability of the electrical path.

The majority of the existing EMSs, regardless of their category or type, are premised upon FC maps or unvarying-parameter mathematical models. In this light, these results remain valid only within a specific operating range. However, the energetic performance of a FC alters by the operating conditions and degradation level variations through the time. Some solutions based on extremum seeking strategies have been proposed to deal with the moving characteristics of the FC systems. The first suggestion is to use the maximum power point tracking methods, such as perturb and observe or hill climbing, to track the real performance of a FC. Such strategies have been used in [32-34] for EMS purposes due to their convenient implementation. However, these methods are not very suitable for simultaneous identification of several characteristics, such as maximum power and efficiency points, in online applications since they require a separate search stage for each feature extraction. The second solution is the use of a parameter identification method coupled with an optimization algorithm. The identification is performed by using an online parameter estimation method and a grey/black box model [35]. Although the black box based strategies are easily applicable in real-time situations, they do not provide any insights into the physical phenomena inside the FC and might become unreliable in case of confronting new situations. Moreover, the analysis of the results become more difficult with black box models due to the ambiguous input-output relationships. In this regard, the employment of semi-empirical models has come under attention. These models contain meaningful physical parameters, which enable a FC expert to analyze the results conveniently. In [36, 37], a semi-empirical FC model, which is only based on current, is utilized and its parameters are identified by

means of recursive filters to update the states of the FC and an optimization algorithm is then employed to find the operating points. The main idea in this line of work is to update the semi-empirical model parameters by means of a recursive algorithm and then apply the EMS. Combining the operating point tracking with the EMS design has been able to improve the performance of a single-stack fuel cell system, as reported in [38]. In this regard, this concept seems to be worthwhile to be tested in the MFCSs.

With respect to the reported manuscripts, it is clear that the use of real-time techniques in the design of adaptive EMSs to respect the real behavior a PEMFC in a MFCS demands more attention. Several online and real-time EMSs for the application of FCVs can be found in the literature. However, the majority of these works deal with single-stack systems. Even, among the existed real-time single-stack EMSs, only few of them have tried to consider the real characteristics of the PEMFC while designing the EMS. Another worth mentioning point is that most of the existent investigations of PEMFC behavior lack the experimental validation.

1.3 Objective

The conducted literature study has disclosed the fact that a MFCS has several advantages over a single-stack system, such as increased efficiency, modularity, and degraded mode operation. However, benefiting from these advantages requires a suitable EMS design to provide the basis for using them. One of the most important factors to have such a strategy is to incorporate the real-behavior tracking of a PEMFC, which goes under performance drifts due to various reasons such as degradation and operating conditions variations, into the EMS design. In this regard, the principal objective of this work is to propose a new adaptive state machine based EMS for a MFCS with a parallel configuration, as shown in Figure 1.3. The

MFCS of this work is composed of four PEMFCs, and a battery pack, which is mainly responsible for absorbing the peaks. The PEMFCs are connected to the DC bus individually by a DC-DC converter to increase the system redundancy. This strategy is indeed an online model based power-sharing methodology premised on a state machine algorithm. The state machine algorithm distributes the power among the PEMFCs and the battery pack. In the meantime, the strategy keeps track of the PEMFCs state of health by determining the present maximum power point of each. In case of detecting maximum power drifts in the PEMFCs, the strategy changes the order based on which it demands power from each PEMFC. It should be noted that the online modeling is performed by using an adaptive filter to update the parameters of a semi-empirical PEMFC model.

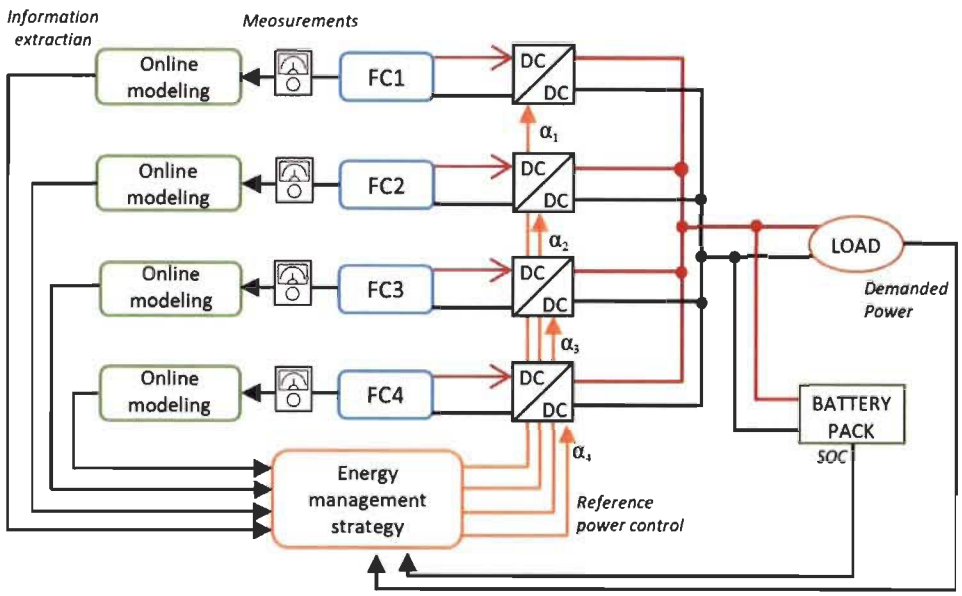

Figure 1.3 MFCS configuration along with the EMS demonstration

1.4 Methodology

A three-step methodology has been followed to complete this thesis. The first step is to review the literature to provide state-of-the-art information about the proposed topic. In this regard, the recent works mainly in the area of EMS designs have been scrutinized, and the areas which are in need of more attentions have been discovered. These gaps have formed the chief objectives of this project, discussed in the previous section. In this regard, a new adaptive state machine based EMS is put forward for the presented MFCS in Figure 1.3.

The second step of this work deals with the development of a suitable PEMFC model for the EMS design. This step comprises two important parts. The first part copes with proposing a simple static online model to track the behavior of the real PEMFC. To do this, Kalman filter has been used to update the parameters of a PEMFC semi-empirical model. The second part of this step is about developing an emulator to imitate the behavior of a real PEMFC. The main reason for designing an emulator is to be used in the hardware-in-the-loop (HIL) simulation for validating the EMS.

The last step of this work is designing an EMS for a MFCS. The proposed EMS of this work has two layers. The first layer is responsible for updating the semi-empirical model and the second layer distributes the power among the energy sources, which are four PEMFCs and a battery pack. It should be noted that as opposed to most of the existing EMS design researches, the results of this work have been validated by implementing the proposed strategy on a developed HIL in the Hydrogen Research Institute (IRH). HIL, which includes the insertion of real components in the simulation loop, is a beneficial step to develop new EMS to test the control limitations and components restraints. Since developing a complete multi-stack PEMFC test bench is expensive, HIL emulator is used to validate the efficiency

of the proposed EMS. Figure 1.4 presents the utilized HIL simulation in this work. As it can be seen, it is composed of a real PEMFC, which is an open cathode 500-W Horizon PEMFC, three PEMFC emulators, which will be discussed in Chapter 2, a battery mathematical model, and four simulated DC-DC converters.

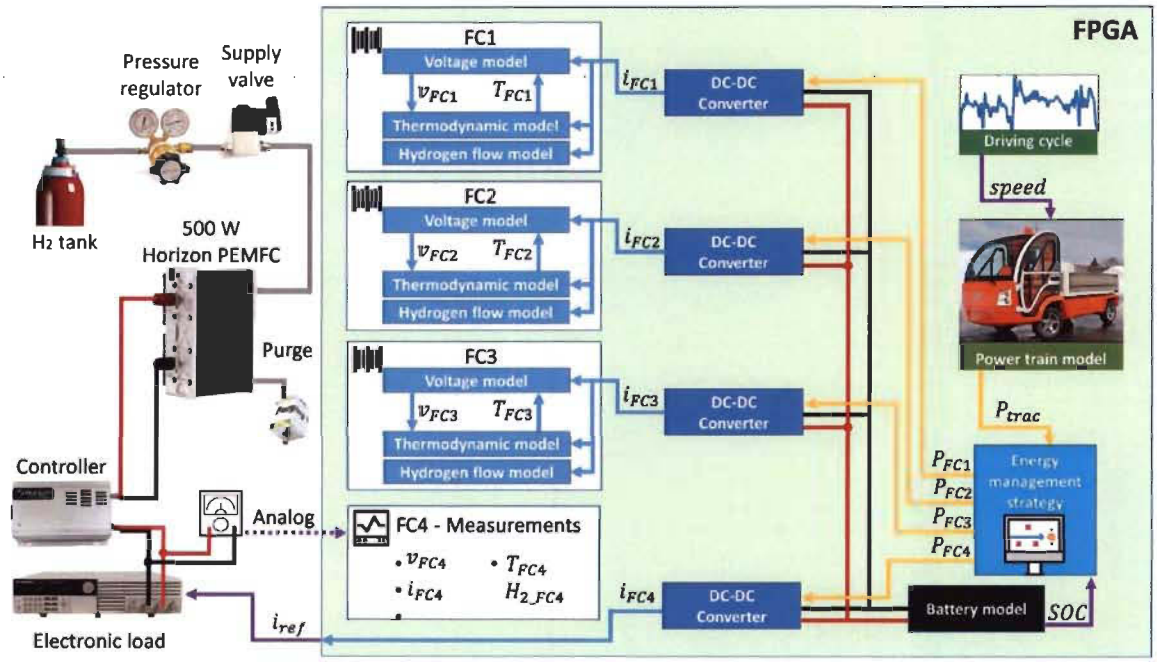

Figure 1.4 The full-scale HIL

1.5 Thesis outline

The rest of this document is organized as follows. Chapter 2 reviews the PEMFC modeling methods, along with a detailed discussion of PEMFC online modeling and emulator design. Chapter 3 provides data on the suggested adaptive EMS and MFCS structure of this work. Chapter 4 investigates the obtained results of simulation and implementation stages. Finally, the conclusion is given with some suggestions for future steps concerning this work in Chapter 5.

Chapitre 2 - Modeling and Online Identification of a Fuel Cell System

2.1 Introduction

Mathematical modeling plays a key role in the technical development of PEMFCs since it can unveil a number of features about the performance of the device and how to enhance it. Generally, PEMFC modeling methods can be fallen into two categories of steady-state and dynamic. Each category has its own advantages, disadvantages, and more importantly its own application. Depending on the application, one chooses the suitable group. Regarding the EMS design, which is the main focus of this work, steady-state models are usually used to devise the strategy [39]. This choice is firstly due to the fact that fuel cell system has a slow dynamic and will be exposed to steady demanded power. Secondly, in hybrid systems, the energy storage devices, such as battery, usually deals with the high dynamic. Therefore, a suitable PEMFC steady-state model needs to be selected for the purpose of EMS design in this work. However, since the proposed EMS of this work is an adaptive strategy based on recursive filters, the filters need a reference input signal to update the steady-state model parameters. In this regard, an emulator, which is a dynamic PEMFC model, needs to be designed to provide the filters with the necessary inputs.

This chapter starts with providing the information on the utilized fuel cell system, which is a low speed vehicle. Subsequently, it outlines the selection of a steady-state model along with the integration of an adaptive filter to update the model online. Then, the obtained results of online modeling are discussed. Moreover, the development of an emulators is described

in details and the outcomes are evaluated. This chapter finishes by giving a synopsis of the main points of each investigated section.

2.2 Power train model

In this work, the developed HIL emulator can be considered as a full scale HIL emulator for Nemo vehicle, which is a laboratory-scale vehicle. The specifications of this vehicle are listed in Table 2 1 .

Table 2-1 Vehicle specification [40]

Dimension	
L: W: H	3.48 m: 1.52 m : 1.90 m
Tire	175/70 R13
Weight	896 kg
Max Load	453 kg
Driving performance	
Maximum speed	40 km/h
Acceleration	6.5s (0-40 km/h)
Autonomy	115 km
Transmission	
Engine	ACX-2043; 4.8kW
Transmission	12; 44:1
Batteries	
Battery series	9x US 8VGCHC XC2
Battery Type	Lead-acid deep cycle
Battery charger	1.3 kW

The requested power from the traction system has been estimated by the following power train model using the driving cycle speed v as the input [40].

$$P_{trac} = (F_{acc} + F_r + F_{ad} + F_{cr}) * v \tag{2.1}$$

Where F_{acc} is the acceleration force, F_r is the friction of the tires, F_{ad} is the aerodynamic drag resistance, and F_{cr} is the resistance of climbing. For this case, it has been assumed that the vehicle is on a flat area and both of the friction and drag resistance are uniform and constant.

The friction of the tire is calculated by:

$$F_r = C_{rr} * m_{total} * g * \cos \alpha_{slope} \tag{2.2}$$

Where C_{rr} is the coefficient of friction (0.015), m_{total} the total mass of the vehicle (896 kg), g is the standard acceleration due to gravity ($9.81\ m/s^2$), and α_{slope} is the slope of the road (0°). The drag force caused by the airflow is calculated by the following equation, which only considers a uniform contacting surface.

$$F_{ad} = 0.5 * \rho_{air} * C_x * A_{aero} * v^2 \tag{2.3}$$

Where ρ_{air} is the air density ($1.2\ kg/m^3$), C_x is the drag coefficient (0.42), A_{aero} is the contact surface area ($4\ m^2$), and v is the vehicle speed (km/h). The acceleration force is calculated by multiplying the acceleration of the vehicle (a_{cc}) by the total mass (m).

$$F_{acc} = a_{acc} * m \tag{2.4}$$

After calculating the requested power (P_{trac}), it is sent to the energy management strategy block. The first thing which is checked in this block is the battery SOC. If the battery needs to be charged, one PEMFC with its maximum power will be allocated to recharge the

battery pack. It should be noted that a hysteresis strategy has been used for the battery pack to keep the SOC level between 50 % and 95 % [41].

2.3 Battery and DC-DC converter models

A simple electric circuit based battery model is used to describe the battery pack of Nemo vehicle [42]. Figure 2.1 shows the equivalent circuit, which is composed of a configuration of series resistor (R_1) and a parallel resistor (R_2) with a capacitor (C) [42].

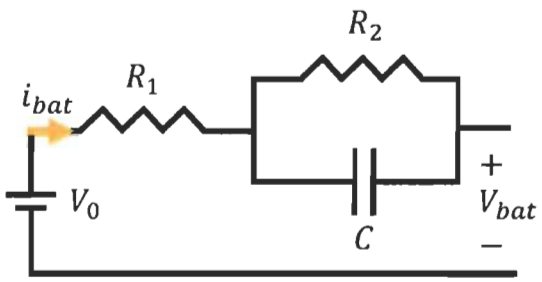

Figure 2.1 Battery equivalent circuit

The current in the circuit is expressed by:

$$i_{bat} = \frac{V_0 - R_1 i_{bat} - V_{bat}}{R_2} + C\frac{d}{d_t}(V_0 - R_1 i_{bat} - V_{bat}) \quad (2.5)$$

where V_0 is the open circuit voltage. The SOC of the battery is calculated by using the initial charging state (SOC_{ini}), current of the battery (i_{bat}), and the capacity of the battery (Q_r=183 Amp h) [43].

$$SOC = SOC_{init} + \frac{\int i_{bat} dt}{3600 * Q_r} \quad (2.6)$$

Since the battery and FCs are connected in parallel to the power transmission, the current flow in the bus is obtained by:

$$i_{bat} = i_{ts} - \sum_{k=1}^{4} i_{FC_k} \quad (2.7)$$

As the PEMFCs are low-voltage and high-current suppliers, the use of converter has been opted to boost the voltage output. Indeed, the converter is used to control the FC current. The inductance response is represented by:

$$i_{L,conv} = \frac{1}{L_{conv}} \int \left(v_{bat} - v_{conv,out} \right) dt \tag{2.8}$$

where $i_{L,conv}$ is the current through the inductor, L_{conv} is the inductance value, and $v_{conv,out}$ is the output voltage of the converter. The output converter voltage is formulated by:

$$v_{conv,out} = m_{fc} v_{bat} \tag{2.9}$$

$$i_{conv,out} = m_{fc} i_{fc} \eta \tag{2.10}$$

where m_{fc} is a gain and the efficiency of the converter (η) is 95%.

2.4 PEMFC modeling

The existing PEMFC models in the literature can be categorized into three groups of white box, known as mechanistic, black box, and grey box, known as semi-empirical, as shown in Figure 2.2 .

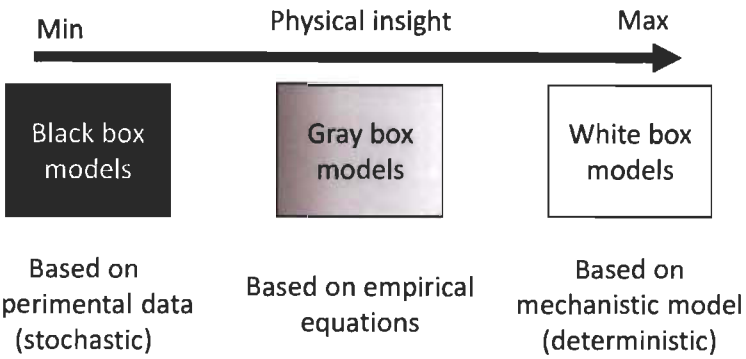

Figure 2.2 PEMFC model categories

Mechanistic models mainly focus on clarifying the phenomena happening inside a single cell and are based on algebraic and differential equations. These equations describe the occurred processes related to thermodynamics, electrochemistry, and fluid mechanics. Mechanistic models require a wide knowledge of influencing parameters such as transfer quantities, humidity level, membrane thickness, etc. to mimic the behavior of the PEMFC over different operating conditions. However, fuel cell is a multiphysics system and a number of factors, such as degradation and operating condition fluctuation, can cause performance drifts in this system. In this regard, design of a complete mechanistic model considering all of the performance drifts is very difficult, time-consuming, and still a study limitation. As opposed to the mechanistic models, black box models are based on inputs and outputs data without any information about the internal workings and physical interpretation of the parameters. Since the computational time of black box models is very low, they have been used in many studies for online vehicular applications. However, the dependability of such models decreases when facing new operating conditions, which have not been included in their training process. The last category of PEMFC modeling belongs to the semi-empirical methods, which are considered as an intermediary between mechanistic and black box types. Semi-empirical models are usually formed by combining the physical relationships with some experimental data. They describe the electrochemical behavior of a PEMFC by imitating the polarization curve, which is a useful approach for both single cell and stack modeling. One of the practical applications of PEMFC semi-empirical models is in the field of EMS design. As mentioned before, these models provide remarkable data on the polarization curve effects, such as cell reversible voltage, and activation, ohmic, and concertation voltage drops, which are very useful to investigate the relevance of the results for fuel cell researchers. Moreover, by having the polarization curve, extracting the power

curve will be very convenient and it can be used in the design of an EMS. Semi-empirical models can also become adaptive easily, which will be discussed hereinafter.

2.4.1 Semi-empirical model

In the light of the explained PEMFC modeling methods in the previous section, semi-empirical models seem to be fitted for EMS purposes. Several semi-empirical models can be found in the literature [44-46]. Among them, the model proposed by Amphlett et al. has been suggested for EMS purposes in a number of different manuscripts. This model has a good mechanistic background, so it has been used in many studies [35, 39]. The other available semi-empirical models may also perform the same as this model, however, they have not had this wide application in the literature.

The proposed electrochemical PEMFC model by Amphlett et al. is for a number of cells connected in series and assumes the same behavior for all the cells. In this model, the output voltage of the PEMFC (V_{FC}) is perceived as the sum of the reversible cell potential (E_{Nernst}) and three voltage drops, namely activation (V_{act}), ohmic (V_{ohmic}), and concentration (V_{con}). The general formulation of this model can be given by:

$$V_{FC} = N(E_{Nernst} + V_{act} + V_{ohmic} + V_{con}) \qquad \mathrm{V_{FC}} = \mathrm{N(E_{Nernst} + V_{act} + V_{ohmic} + V_{con})} \tag{2.11}$$

where N is the number of cells, and the unit of V_{FC} is volt. E_{Nernst} is calculated based on the following theoretical formula:

$$E_{Nernst} = 1.229 - 0.85 \times 10^{-3}(T - 298.15) + 4.3085 \times 10^{-5}T[\ln(P_{H2}) + 0.5\ln(P_{O2})] \tag{2.12}$$

where T is the stack temperature (K), P_{H2} is the partial pressure of hydrogen in anode side (atm), and P_{O2} is the partial pressure of oxygen in cathode side (atm). V_{act} is obtained by:

$$V_{act} = \xi_1 + \xi_2 T + \xi_3 T ln(CO_2) + \xi_4 T ln(i)$$

(2.13)

where $\xi_n (n = 1 \dots 4)$ are semi-empirical parameters based on fluid mechanics, thermodynamics, and electrochemistry, CO_2 is the oxygen concentration (mol cm^{-3}), and i is the PEMFC actual current (A). The oxygen concentration is calculated by:

$$CO_2 = \frac{P_{O2}}{5.08 \times 10^6 \exp(-498/T)}$$

(2.14)

The computation of the V_{ohmic} is based on (2.5), where $\zeta_n (n = 1 \dots 3)$ are the parametric coefficients. This way of ohmic loss formulation has a considerable structure to avoid requiring specific information for calculation of water content or membrane thickness.

$$V_{ohmic} = -iR_{internal} = -i(\zeta_1 + \zeta_2 T + \zeta_3 i)$$

(2.15)

It should be noted that ohmic loss formulation is a function of temperature, mainly due to the fact that diffusivities and water partial pressures vary with temperature, and current, because proton and water fluxes change with the current. Finally, V_{con} is given by:

$$V_{con} = Bln(1 - \frac{J}{J_{max}})$$

(2.16)

where B is a parametric coefficient (V), J is the actual current density (A cm^{-2}), and J_{max} is the maximum current density (A cm^{-2}).

The discussed electrochemical PEMFC model has eight parameters to be identified, which are listed in Table 2 1 . As previously discussed, a PEMFC system experiences some performance drifts during its lifetime. These drifts are because of degradation phenomenon, which happens slowly over time, and the influence of conditions which are not included in the model such as humidity. In order to take these effects into account, the model parameters need to be updated online to adapt the model to the real state of the PEMFC system. The reported ranges of the listed parameters in Table 2-1 have been collected from the available researches in the literature [35, 47]. That is to say, using a proper initial value is necessary for having satisfactory results while using the adaptive filters, especially when some of the model parameters have physical interpretations. In this regard, a preprocessing of data is suggested to avoid a long convergence time or divergence in the parameters and to get close to realistic results. The pre-treatment is performed by the Curve Fitting Toolbox™ of MATLAB software. This toolbox uses the least square methods to fit the data. Fitting requires a parametric model, which can relate the real data to the predictor data. In this work, the employed fuel cell model is linear in coefficients. The least square method minimizes the summed square of the difference between the observed and the estimated value. The employed experimental data in the preprocessing stage comes from the conducted test for obtaining the polarization curves of the fuel cells, which is a proper representative of its behavior. This initialization method has shown that it can reach stable parameters in 400 seconds [47]. This time is acceptable for the FC application, since the variations in the performance of the FC are slow (in order of hours).

Table 2-1 The unknown parameters of the semi-empirical model

Parameter	Minimum	Maximum	Reference
ξ_1	-1.997	-0.8532	[35]
ξ_2,	0.001	0.005	[35]
ξ_3	$3.6\text{x}10^{-5}$	$9.8\text{x}10^{-5}$	[35]
ξ_4	$-2.6\text{x}10^{-4}$	$-0.954\text{x}10^{-4}$	[35]
ζ_1			[47]
ζ_2	Current interrupt test		[47]
ζ_3			[47]
B	0.0135	0.5	[35]

2.4.2 Resistor measurement

In this work, current interrupt test has been used as an electrochemical technique to obtain a range for the resistor variation with regard to current and temperature [41-44]. This range can be used as reference to validate the estimation result of the internal resistor ($R_{internal}$) of the PEMFC. The practicality of this method for measuring the resistor of a PEMFC stack has been already studied in [47-49]. Current interrupt test measurement is based on the rapid acquisition of the measured voltage, after interrupting the current in the PEMFC. The fast data acquisition is necessary to separate the ohmic loss from the activation loss, which disappears faster than electrochemical losses after current interruption. Therefore, the ohmic loss can be obtained from the difference between the voltage measurement immediately before and after the interruption.

In this work, the steps for conducting the current interrupt test is completely pursuant to [47]. One of the main advantages of the current interrupt test compared to other electrochemical methods is the straightforward result analysis. However, the measurement needs to be done with a fast oscilloscope to exactly catch the point in which the voltage jumps.

Table 2-2 presents different current levels and their corresponded temperature in which the interruption test has been performed. It should be noted that the PEMFC has been allowed enough time to achieve a stable temperature for each current level before doing the test. The current interrupt test has been performed in a forced convection condition where the fans of the PEMFC worked with a constant duty cycle of 34%.

Table 2-2 Current levels and PEMFC stack temperature during resistor measurement

Current (A)	Temperature (°C)
3	23.2
6	25
9	26.25
12	28.2
15	30.9
18	33.7
21	38.15
24	44.7
25	49.4

Figure 2.3 indicates the change of the resistor with regard to current and temperature for the utilized PEMFC. As mentioned before, this measurement is used as a reference to check the range of the estimated resistor by the identification algorithm.

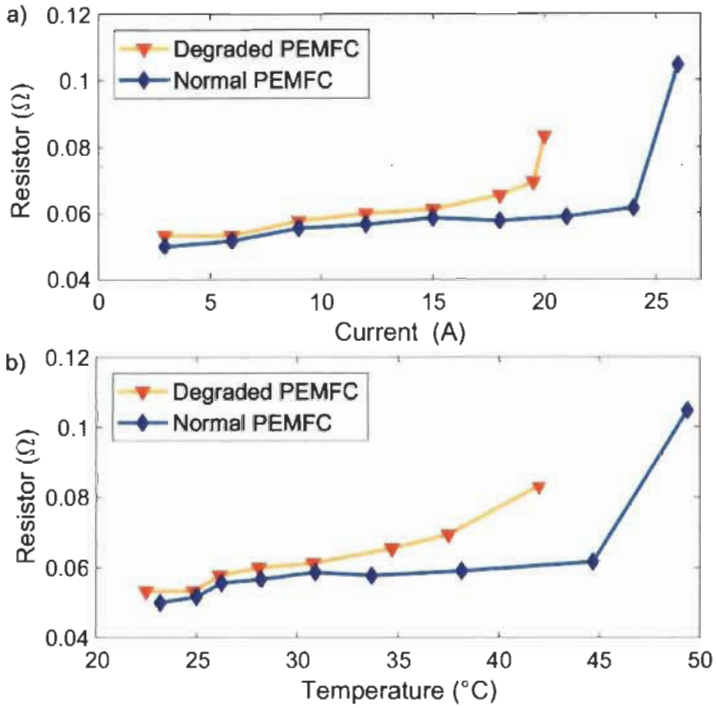

Figure 2.3 Evolution range of the PEMFC internal resistor with respect to current (a) and temperature (b) [47]

2.4.3 Online parameter identification

Generally, the identification process can be performed offline and online, as shown in. In Figure 2.4 offline identification, the measured data is first saved in a data storage and then it is transferred to a computer for further analysis and evaluation. This type of identification is conducted by using batch processing of the data, which means assessing the complete data at once. Direct identification techniques, like least squares, are usually used for this type of identification. In online identification, the process is done through an online operation and the data is evaluated immediately after each sample is collected. Recursive identification

algorithms are used in online processes, which means that no data storage is required in online identification. In this work, online parameter identification is in demand. It is mainly due to the fact that, as mentioned before, the parameters of a PEMFC model are time-varying. Since the PEMFC performance is affected by degradation and operating conditions, updating the model parameters is necessary. Kalman filter and recursive least square (RLS) are two well-known recursive filters, which have been successfully used in different engineering problems. In [35], the robustness of RLS has been investigated and realized that its performance decreases when facing noisy data. In [35], the performance of Kalman filter and recursive least square have been compared in the PEMFC model parameter estimation problem and concluded that Kalman filter benefits from more robustness. In this regard, the focus of this section is to use Kalman filter to identify the parameters of the introduced electrochemical PEMFC model online.

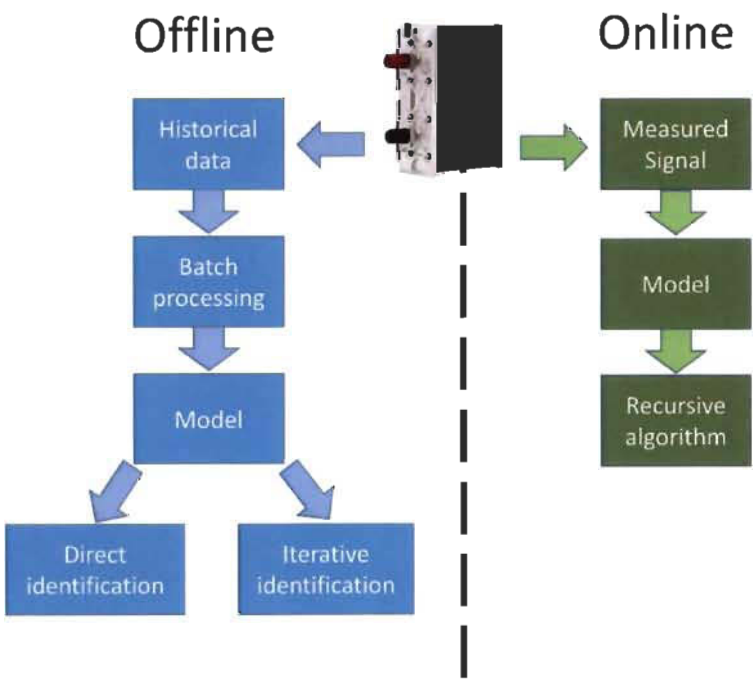

Figure 2.4 Different ways of processing the measured data in identification process

Kalman filter is considered as an optimal estimator and it can estimate the parameters of interest from imprecise and uncertain observations. Figure 2.5 shows the process of integrating Kalman filter into the parameters estimation of the PEMFC model.

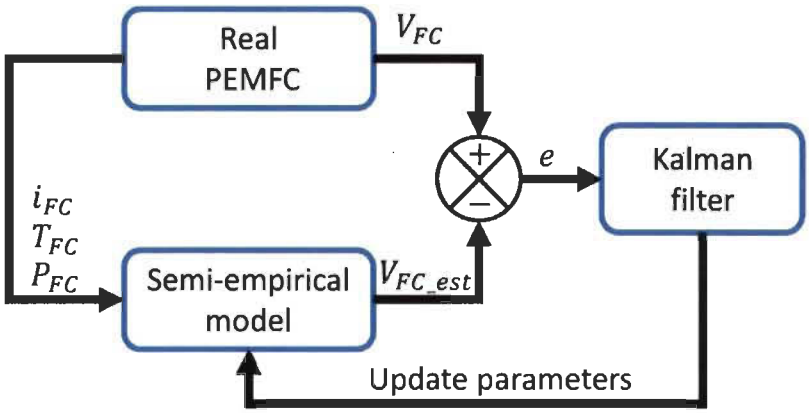

Figure 2.5 Online PEMFC modeling procedure

Kalman filter identifies the current state parameters first and then updates them when the next measurement is received. The structure of Kalman filter is as follows:

$$\begin{cases} x(t+1) = F(t+1|t)x(t) + w(t) \\ y(t) = H(t)x(t) + v(t) \end{cases} \text{ (steady-state model)} \quad (2.17)$$

$$\hat{x}^-(t) = F(t|t-1)\hat{x}^-(t-1) \text{ (steady-state propagation)} \quad (2.18)$$

$$P^-(t) = F(t|t-1)P(t-1)F^T(t|t-1) + Q(t-1) \text{ (Error covariance propagation)} \quad (2.19)$$

$$G(t) = P^-(t)H^T(t)[H(t)P^-(t)H^T(t) + R(t)]^{-1} \text{ (Kalman gain matrix)} \quad (2.20)$$

$$\hat{x}(t) = \hat{x}^-(t) + G(t)(y(t) - H(t)\hat{x}^-(t)) \text{ (State estimate update)} \quad (2.21)$$

$$P(t) = (I - G(t)H(t))P^-(t) \text{ (Error covariance update)} \quad (2.22)$$

where t is the discrete time, $x(t)$ is the state vector, which is unknown and here it can be called parameters vector as well, $\hat{x}(t)$ is the estimate of the state vector, $\hat{x}^{-}(t)$ denotes priori estimate of the state vector, $F(t+1|t)$ is the transition matrix, which takes the state vector from time t to time $t+1$, $w(t)$ is the process noise, $y(t)$ is the output, $H(t)$ is the measurement matrix, $v(t)$ is the measurement noise, $P(t)$ is the error covariance matrix, $Q(t)$ is the process noise covariance matrix, $G(t)$ is the Kalman gain, $R(t)$ is the measurement noise covariance matrix, and I is the identity matrix. Table 2 3 shows the customization of the explained Kalman filter for the problem of PEMFC model parameter estimation. As it can be seen in this table, state vector is composed of the targeted parameter for the identification, and the measurement vector is in fact the coefficient of each parameter in the introduced PEMFC formulation. It should be noted that the transition matrix has been assumed to be an identity matrix, which means that the future state is guessed to be the same as the current state and the error will be compensated by the filter.

Table 2-3 Kalman filter customization for the identification problem

Kalman operators	Symbols	Implementation description
State vector	$x(t)$	$[\xi_1, \xi_2, \xi_3, \xi_4, \zeta_1, \zeta_2, \zeta_3, B]$
Measurement vector	$H(t)$	$[1, T, Tln(CO_2), Tln(i), -i, -iT, -i^2, ln(1 - \frac{J}{J_{max}})]$
Measured output	$Y(t)$	Measured V_{FC} from the real PEMFC
Transition matrix	$F(t+1\|t)$	Identity matrix

2.4.4 Results and discussion

The performance assessment of the explained online modeling procedure is detailed in this section. In order to test the performance of this parameter identification process, the explained semi-empirical model with the Kalman filter have been implemented in a developed test bench in Hydrogen Research Institute (IRH) of Université du Québec à Trois-Rivières. This test bench is represented in Figure 2.6 . As it can be seen in this figure, this test bench comprises a Horizon H-500 air breathing PEMFC which is connected to a National Instrument CompactRIO through its controller. A 8514 BK Precision DC Electronic Load is used to ask load profiles from the open cathode PEMFC. According to the manufacturer, the difference between the pressure of the PEMFC in the anode side and the atmospheric pressure in the cathode side should be kept around 50.6 kPa. The pressure in the anode side is set to 55.7 kPa. The explained semi-empirical model and parameter identification method has been first designed and initialized in MATLAB and then put into Lab VIEW software via Math Script Module. A current load is applied to the PEMFC by using the programmable DC Electronic Load, which communicates with LabVIEW software and PC through a USB connection. The measured temperature and voltage from the open cathode PEMFC are sent to the PC with the help of the CompactRIO. The measured data are used in the implemented model for testing the identification process. The information between CompactRIO and the PC is transferred by means of an Ethernet connection every 100 milliseconds. In this respect, it can be stated that Kalman filter receives the measured data very 100 milliseconds and update the parameters of the model before the next measurement arrives. Then the updated model can be used for extracting useful information, such as maximum power and maximum efficiency, to be used in the EMS design. After extracting the required information from the

updated model, the current that leads to the maximum efficiency/power can be requested from the PEMFC via the electronic load.

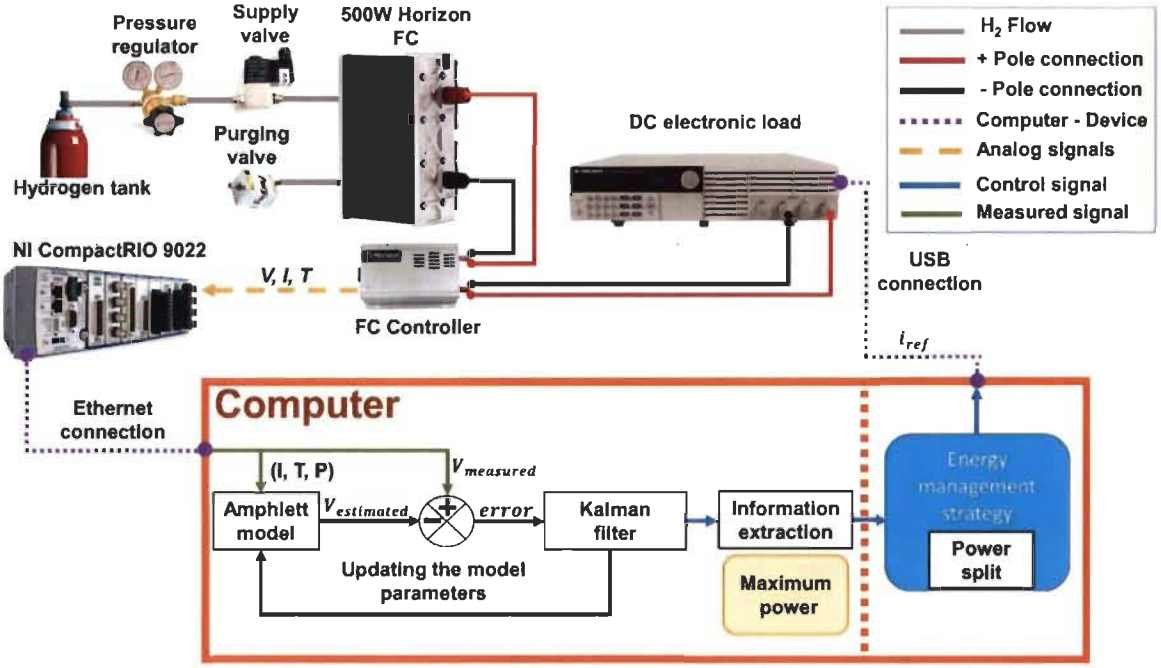

Figure 2.6 The employed set up for testing the online modeling

Figure 2.7 presents the current profile and the corresponded measured voltage and temperature of the PEMFC. This current profile has been extracted from the UDDS driving cycle, which represents the urban driving condition. The extraction of the demanded load profile from the UDDS driving cycle has been done by means of the IEEE VTS Motor Vehicles Challenge Simulink file available in [50], and the obtained required current from the PEMFC has been scaled within the operating range of the employed PEMFC in the test bench. In Figure 2.7 subplot c) indicates the comparison of the estimated voltage by the online modeling with the measured voltage of the PEMFC. As it is observed, the proposed online model is able to estimate the voltage with a satisfying precision. Figure 2.8 compares the obtained polarization curve and power curve of the online model with curves of the real

PEMFC. According to this figure, the model can predict the maximum power and polarization behavior of the PEMFC with an acceptable accuracy. It should be noted that for each case of prediction the mean square error (MSE) has been reported in the caption of the figures to clarify more the estimation quality. MSE shows the cumulative squared error between the estimated voltage and the measured voltage. The lower the value of MSE, the lower the error.

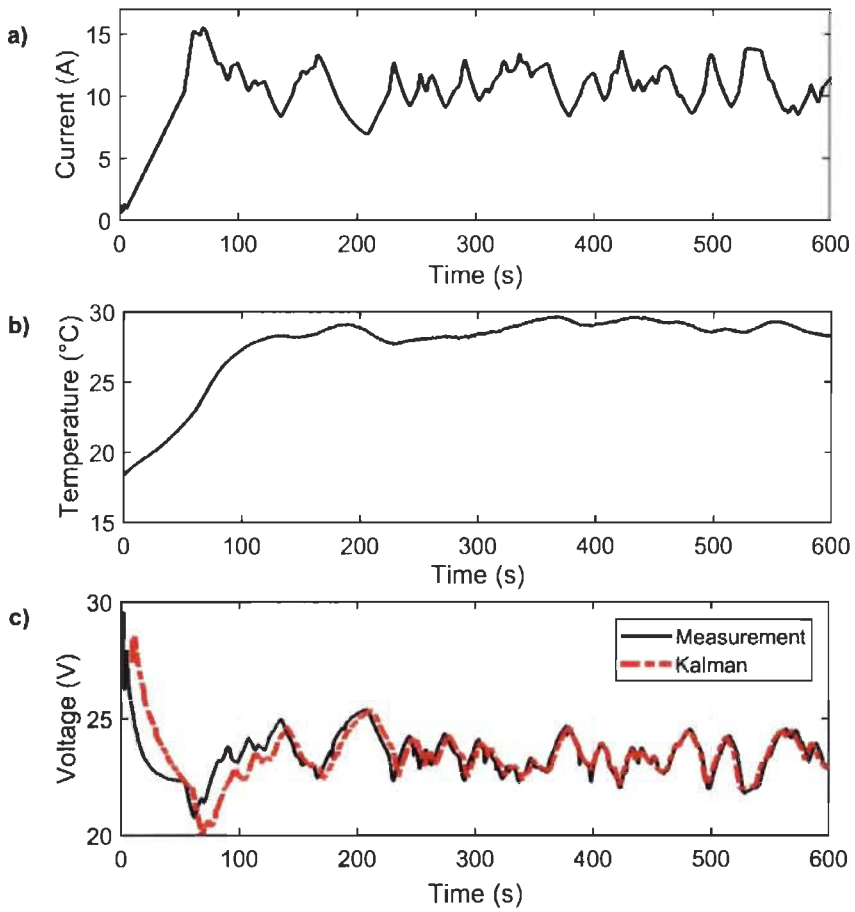

Figure 2.7 The voltage estimation result. a) Applied current profile to the PEMFC system, b) Measured temperature, c) Comparison of measured and estimated voltage (MSE: 0.1475)

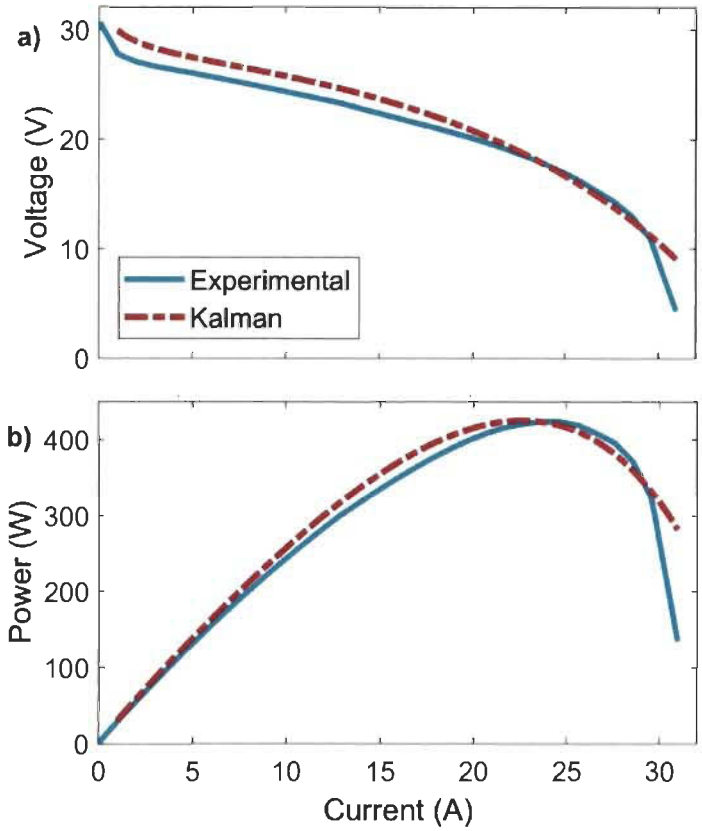

Figure 2.8 Polarization curve a) and Power curve b) for the experimental and estimated curves by mean of Kalman filter with a MSE of 3.44 (by using the extracted parameter at 200 s)

Figure 2.9 represents the prediction of the value for internal resistor of the PEMFC. The resistor seems to be in the same range obtained by the current interrupt test and it is a promising indication for validating the estimation of this physical parameter. It should be noted that the observed increase in the resistor evolution specifically between 0 to 100 is because of the utilized current profile to test the estimation. In the utilized profile, shown in Figure 2.7 , the current profile undergoes a sudden growth which results in a temperature increase influencing the resistor evolution. As previously-mentioned the internal resistor is affected by operating current and temperature. Table 2-4 shows the average value of

activation and concentration drop related semi-empirical parameters. It should be noted that the achieved parameters in this work are almost in the same range as in Table 2 4 , which have been collected from other manuscripts in the literature. The subtle difference in some of the parameters is probably attributable to different aging and conditions of the PEMFC systems from which the data has been obtained.

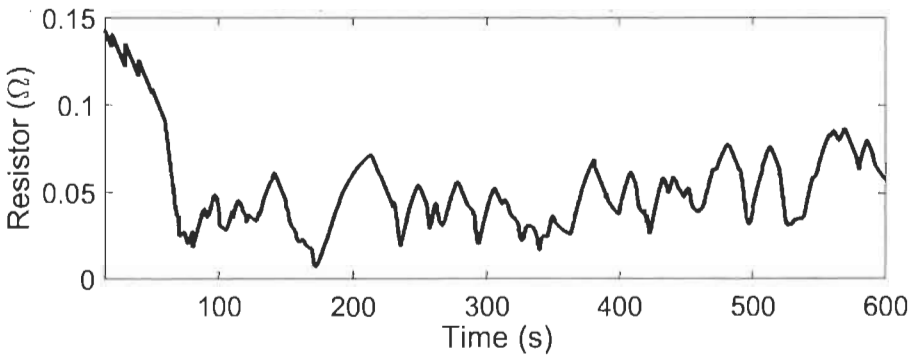

Figure 2.9 PEMFC internal resistor evolution

Table 2-4 Average value of the estimated parameters (activation and concertation)

Parameter	Obtained value	Minimum	Maximum
ξ_1	-1.29	-1.997	-0.8532
ξ_2	0.0032	0.001	0.005
ξ_3	1.3×10^{-5}	3.6×10^{-5}	9.8×10^{-5}
ξ_4	-0.952×10^{-4}	-2.6×10^{-4}	-0.954×10^{-4}
B	0.351	0.0135	0.5

Figure 2.10 shows the change of the activation region parameters of the PEMFC with Kalman filter. As it can be seen in this figure, the parameters have some variation and this small variation of the parameters overtime implies that the selected PEMFC model has an acceptable accuracy, otherwise the parameters would fluctuate a lot to compensate the lack of accuracy in the model. The fluctuation of the concentration loss parameter, achieved by Kalman filter, is shown in Figure 2.11 . It should be reminded that although the influence of degradation on each parameter is not clear, the estimation process assures that in case of having performance drifts, the parameters change to update the model to the new condition.

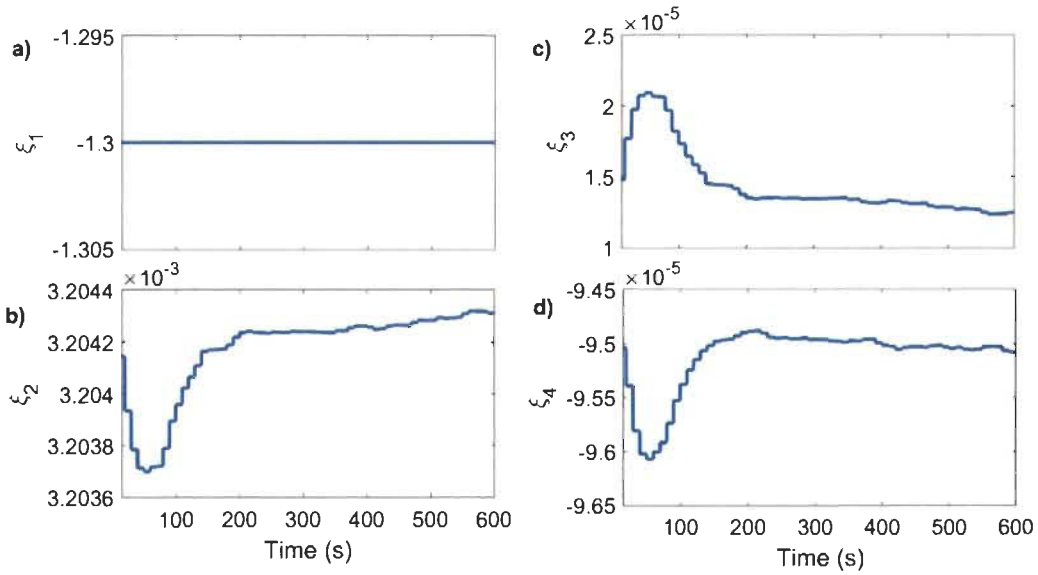

Figure 2.10 The fluctuation of the activation loss parameters

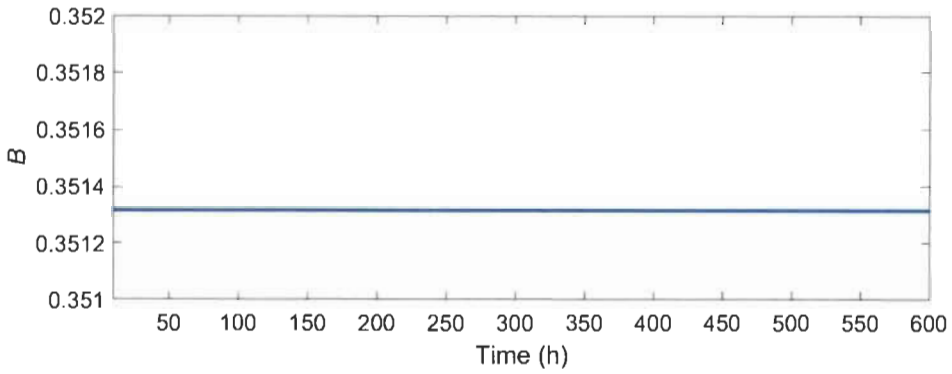

Figure 2.11 The variation of the concentration loss parameter

2.5 Emulator design

Fuel cell technology can be still considered rather young and has not reached its maturity in the market yet. In this regard, PEMFC stack price is still pretty expensive and the required fuel of the PEMFC, which is highly-pure hydrogen, is pricy. Another worth noting aspect about the PEMFC is that exposing PEMFC system to different requesting operating conditions, such as immediate load changes or fast and high current ripples, has detrimental effect on the lifetime of the device and even can cause irreversible damage to the stack. All the above-mentioned factors restrict the utilization of real PEMFCs in new applications especially in power conditioning experiments. Such projects need to be developed and tested first by using emulators which are able to mimic the behavior of a PEMFC. Designing a suitable emulator requires detailed information about static and dynamic features of the PEMFC stack to be able to check the response of the system in critical operating conditions, like maximum achievable power, and rapid load alterations.

Several researchers have worked on the subject of obtaining a precise PEMFC model in the past years. A number of existing manuscripts have focused on extracting the parameters of a static model by means of metaheuristic optimization algorithms. For instance, grey wolf and slap swarm optimizers have been used to estimate the model parameters in [51, 52]. Genetic algorithms and particle swarm optimization have been employed to identify the parameters of another PEMFC stack in [53, 54]. Moreover, some curve fitting techniques such as least squares have been used to extract the parameters of static PEMFC models [55]. However, all the mentioned manuscripts revolve around modeling the static polarization behavior of a fuel cell system and they lack the dynamic characteristics of a fuel cell system, which are vital for investigating the performance of a PEMFC in power systems. Some intelligent model techniques based on fuzzy logic and artificial neural networks can be found in the literature which have been used to model the static and dynamic behavior of a single-stack and even multi-stack PEMFC systems. One of the drawbacks of such modeling techniques is that they are not really appropriate for exploring the electrical and electrochemical behavior of a PEMFC and its interaction with other energy storage devices [56]. Another restricting aspect of generally non-circuital models is the difficulty of their implementation in different simulation environments.

A through survey of selecting criteria of a PEMFC model has been conducted in [57], by considering the commercial models and concluded that equivalent circuit models are the most practical modeling approach for obtaining a realistic interaction between the PEMFC and the load. Furthermore, equivalent circuit models are very useful for power system designs and have been used several times for simulation of energy management and optimization projects. One of the most frequent used models in the literature has been introduced by Larminie et.

al. [58]. However, there are not still any certainties regarding the accurate value of the parameters for each PEMFC stack and this model has been combined and improved in different studies to enhance the performance of the simulation.

The main purpose of this section is to acquire a dependable and accurate model for the 500-W Horizon PEMFC, which has been used in the developed test bench of IRH, to be utilized in hardware-in-the-loop emulator with the aim of investigating the energy management of a hybrid multi-fuel cell system which is composed of four PEMFCs and a battery pack.

2.5.1 Dynamic modeling

The main application of the emulator in this work is for the design of an energy management strategy in a hybrid multi-stack fuel cell system, as stated in the previous section. In this regard, a low-frequency model is adequate in such a system. However, the temperature dynamic, which has a substantial influence on the PEMFC performance while operating at high currents, needs to be taken into account in this emulator. Therefore, this section presents the development and calibration of a PEMFC model to imitate the static and low-frequency behavior of a 500-W Horizon PEMFC in the complete operating temperature of the system.

The model development for the purpose of this work involves formulating the electrochemical and thermal characteristics of a PEMFC. The electrochemical model of this work is based on [44, 58, 59]. The charge double layer effect has been added to the electrochemical model based on the proposed structure in [60]. The thermal behavior of the open cathode PEMFC has been modeled by employing the energy conservation law for a

lumped system, explained in [61, 62]. Figure 2.12 represents the schematic design of the emulator of this work.

The PEMFC output voltage is calculated by:

$$V_{FC} = N(E_{Nernst} + V_{act1} + V_C + V_{ohmic}) \tag{2.23}$$

where V_{FC} is the output voltage (V), N is the number of cells, E_{Nernst} is the reversible cell potential (V), V_C is the double-layer charging effect, V_{ohmic} is the ohmic loss (V), and V_{act} is the activation loss (V). Activation drop is made up of a part related to the PEMFC internal temperature (V_{act1}) and a part associated with the both current and temperature of the stack (V_{act2}).

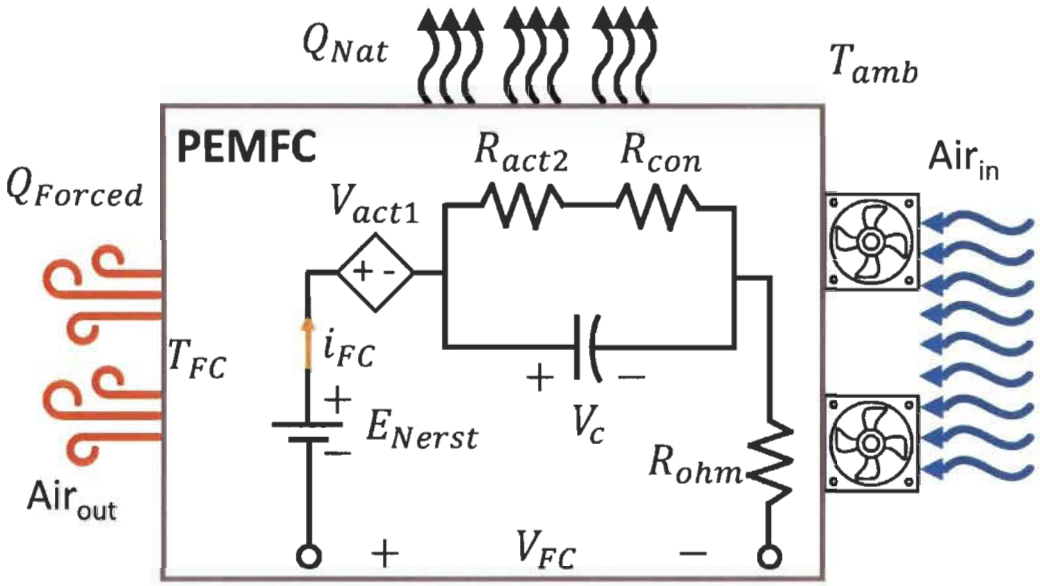

Figure 2.12 The PEMFC system emulator

The reversible cell potential is formulated in the same way as described before in semi-empirical model development section. However, the formal has been written again to

facilitate understanding of the dynamic modeling. Therefore, the reversible cell potential is calculated by:

$$E_{Nernst} = 1.229 - 0.85 \times 10^{-3}(T - 298.15) + 4.3085 \times 10^{-5}T[\ln(P_{H2}) + 0.5\ln(P_{O2})] \quad (2.24)$$

where T is the stack temperature (K), P_{H2} is the hydrogen partial pressure in anode side (atm), and P_{O2} is the oxygen partial pressure in cathode side (atm). The activation loss formulated as:

$$\begin{cases} V_{act} = -[V_{act1} + V_{act2}] \\ V_{act1} = -[\xi_1 + \xi_2 T + \xi_3 T ln(CO_2)] \\ V_{act2} = -[\xi_4 T ln(i)] \\ CO_2 = P_{O2}/5.08 \times 10^6 \exp(-498/T) \end{cases} \quad (2.25)$$

where $\xi_k (\mathrm{k} = 1 \ldots 4)$ are the semi-empirical parameters, CO_2 is the oxygen concentration (mol cm^{-3}), and i is the PEMFC operating current (A). The double-layer charging effect is calculated by:

$$\begin{cases} V_C = (i - c\, dV/dt)(R_{act2} + R_{con}) \\ R_{act2} = V_{act2}/i \\ R_{con} = V_{con}/i = (Bln(1 - J/J_{max})/i) \end{cases} \quad (2.26)$$

where c is the equivalent capacitor due to the double-layer charging effect (F), which is in order of several Farads because of porous electrodes of the PEMFC [58, 60], B is a parametric coefficient (V), J is the actual current density (A cm^{-2}), J_{max} is the maximum current density (A cm^{-2}), and V_{con} is the concentration loss (V). The ohmic voltage drop can be calculated by:

$$V_{ohmic} = -iR_{internal} = -i(\zeta_1 + \zeta_2 T + \zeta_3 i) \quad (2.27)$$

where $R_{internal}$ is the internal resistor (Ω), and $\zeta_k (\mathrm{k} = 1 \ldots 3)$ are the parametric coefficients.

The energy balance for studying the thermal effect in the characteristics of the PEMFC can be formulated by:

$$m_{st} C_{st}\, dT_{st}/dt = \dot{Q}_{reac} - P_{st} - Q_{Nat} - Q_{Forced} \tag{2.28}$$

where m_{st} is stack mass (4.2 kg), C_{st} is specific heat capacity of stack (1260 J/kg K) [62], T_{st} is stack temperature (K), $\dot{Q}_{reac}$ is the released energy from electrochemical reaction (J), P_{st} is the generated electrical power (W), Q_{Nat} is the natural convection (J), and Q_{Forced} is the forced convection (J). The acquired energy form electrochemical reaction and the produced electrical power of the stack is determined by:

$$\dot{Q}_{reac} = V_{max}\, i\, N \tag{2.29}$$

$$V_{max} = \Delta H/nF \tag{2.30}$$

$$P_{st} = V_{FC}\, i \tag{2.31}$$

where V_{max} is the maximum voltage obtained by hydrogen low heating value (1.23 V) or hydrogen high heating value (1.23 V), ΔH is the formation enthalpy, n is the number of electrons per molecule, and F is the Faraday's constant. The heat transfer (convection) is in the form of natural and forced, and is given by:

$$Q_{Nat} = h_{Nat}\, A_{Nat}(T_{st} - T_{ca}) \tag{2.32}$$

$$Q_{Forced} = \alpha\, D_{fan}\, \rho_{air}\, A_{Forced}\, C_p(T_{st} - T_{ca}) \tag{2.33}$$

where h_{Nat} is the natural heat transfer coefficient (14 W/m^{2}K) [61], A_{Nat} is the total surface area of the 500-W Horizon PEMFC (0.1426 m^2) which has been calculated by the available dimensions in the manual of the device, T_{ca} is the ambient temperature (K), α is an empirical coefficient obtained by experiment, D_{fan} is the fan duty factor, ρ_{air} is the ambient air density

($1.267\ \mathrm{kg}/m^3$), A_{Forced} is the area exposed to the forced convection ($0.22\ \mathrm{m} \times 0.13\ \mathrm{m} \times 2$), and C_p is the air specific heat capacity (1005 J/kg K).

The targeted parameters which need to be estimated to calibrate the model are listed in Table 2 5 . These parameters are estimated by the introduced metaheuristic optimization algorithm in the next section. The range of parameters is specified in the listed references in Table 2 5 .

Table 2-5 Targeted parameters for model calibration

	Parameter	Minimum	Maximum
	ξ_1	-2	-0.5
	ξ_2	0.001	0.005
	ξ_3	1×10^{-5}	1×10^{-4}
	ξ_4	-9×10^{-4}	-1×10^{-5}
Electrochemical	c	0.1	10
	B	0.0135	0.5
	ζ_1	1×10^{-3}	9×10^{-3}
	ζ_2	1×10^{-6}	9×10^{-6}
	ζ_3	-9×10^{-4}	-1×10^{-4}
Thermal	α	0.01	0.1

The hydrogen flow is estimated with a first order function based on experimental data. The inputs variables for this model is the current of the FC (i_{FC}) and the duty cycle of the fan (DC) that is set to 34% in this work.

$$H_{2,flow} = a + b * i_{FC} + c * DC \tag{2.34}$$

Since the proposed strategy of this work is an adaptive energy management, it is necessary to take into account the influence of ageing in the modeling part. The main purpose of including the ageing is to show how the proposed adaptive EMS functions when the PEMFCs undergo the performance drifts. In this regard, the effect of degradation has been considered on each parameter of the PEMFC model (voltage model, temperature model, and hydrogen consumption model) by using a polynomial function [63, 64]. The utilized polynomial function for degradation is able to estimate the behavior of the PEMFC during a long test. This second order function, Eq. (2.35), is used for each parameter based on the experimental data, where t represents the time in terms of hours, x_k is the initial value, and x_c the actual one.

$$x_c = a * {x_k}^2 + b * x_k + c * t \tag{2.35}$$

2.5.2 Model calibration

Constrained optimization has become an integral part of many engineering problems. In fact, this kind of problem revolves around defining the mathematical optimization by a number of limitations which form the search space for calibrating the parameters of the problem. Metaheuristic optimization algorithms are often utilized to solve such problems by finding near global solutions. They optimize the problem by iteratively attempting to enhance a set of selected solutions with respect to a predefined measure of quality, which is also

known as cost function. Metaheuristic algorithms are non-derivative methods which use deterministic rules to resolve nonlinear and nonconvex problems.

As stated before, several metaheuristic optimization algorithms have been used for calibration of static and dynamic PEMFC models. Among them, differential evolution (DE) is easy to implement with physical experimental data. DE has been introduced by Rainer Storn in [65]. Basically, it starts working by using a set of initial agents. These agents explore the defined search space by using a straightforward equation to find new positions and better solutions with the hope of obtaining a satisfactory result. Therefore, finding the optimal answer is not guaranteed. Figure 2.13 shows the evolution of the parameter vectors in DE where the location of the parameters gets nearer to the optimal area in each generation.

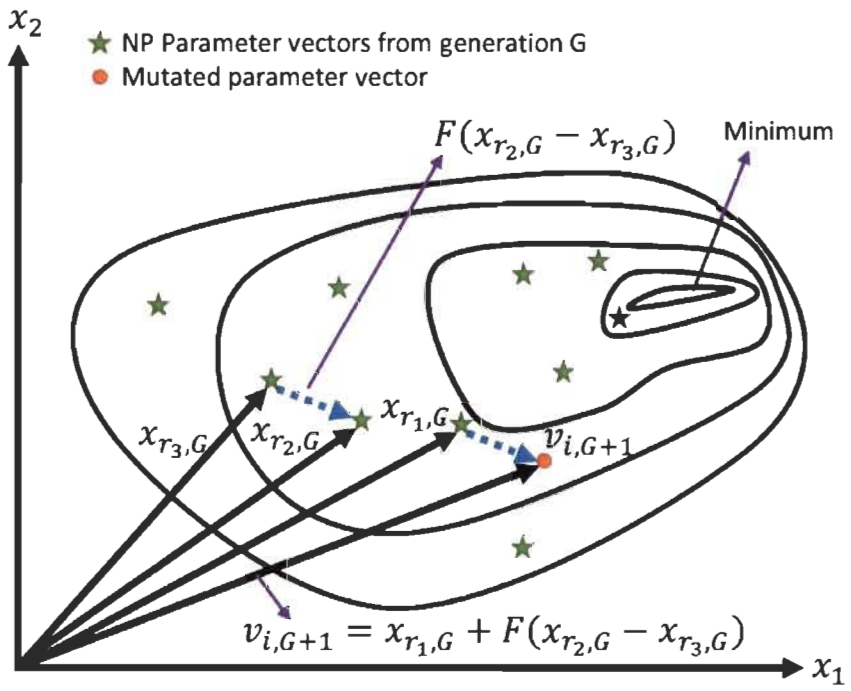

Figure 2.13 DE parameter evolution process for two-dimensional cost function [65]

In order to guarantee that the agents converge to the minimum, the initial population of vectors need to cover the entire search space. DE algorithm is composed of four steps: initialization, mutation, crossover and selection [65]. Figure 2.14 shows the flowchart of DE algorithm. In the initialization stage, the user needs to define the population number (NP). This number should be selected with respect to the number of identifiable parameters to assure the satisfactory performance of the method. In order to reduce the computational time and increase the probability of finding the best answer, a vector with the minimum and maximum values of parameters is defined. This vector also determines the search space. In addition, the user defines the probability of mutation (CR) and an amplification factor for the DE (F). For each vector of population, a mutation procedure is performed. The indexes ($r1$, $r2$, and $r3$), which are mutually different to one another and to the running index I, are selected randomly. Mutation process can be formulated by:

$$v_{i,G+1} = x_{r1,G} + F.(x_{r2,G} - x_{r3,G}) \tag{2.36}$$

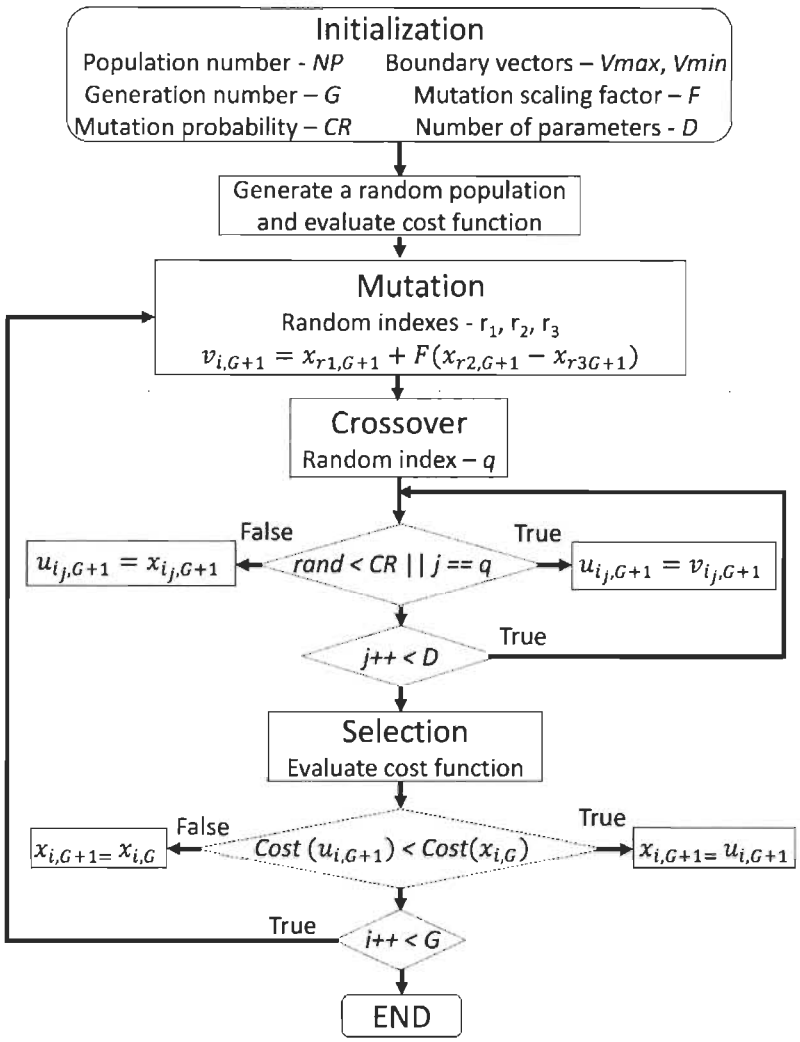

Figure 2.14 DE flowchart

where F is a scaling factor that multiplies the differential variation of two members. As it is shown in Figure 2.13 , this value is added to a third vector to direct the offspring to the optimal solution. The scaling factor has been suggested to be different from the other parameters on the vector to increase the diversity ($F \in [0,2]$). The crossover operator is the combination of the mutation vector with its predecessors. For each parameter, it evaluates a uniform random number between 0 and 1. CR is the crossover probability. To assure that at least one parameter will change, a random index is chosen. Figure 2.15 shows an example of

the crossover phase for a seven-parameter vector. This combination is defined based on the following criteria:

$$u_{i_j,G+1} = \begin{cases} v_{i_j,G+1} & if\ (rand < CR \parallel j == randi[1, NP]) \\ x_{i_j,G+1} & else \end{cases} \tag{2.37}$$

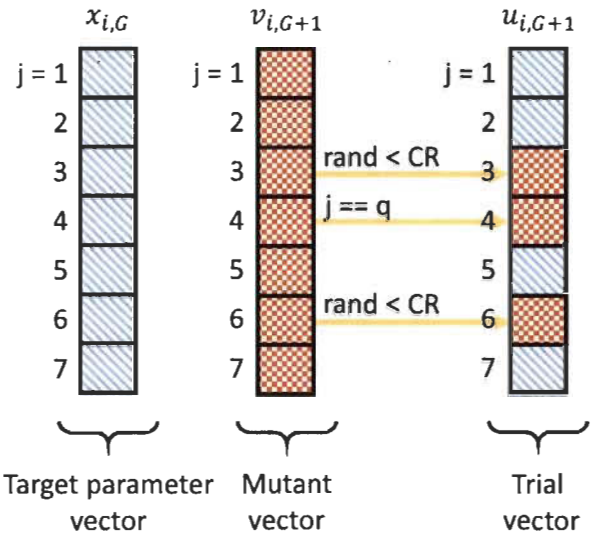

Figure 2.15 Representation of crossover process for seven parameters [65]

The last step of the flowchart deals with the selection of the best found solution. If the latest offspring has a smaller cost function value, it will be set as the new parent vector, otherwise the old one is used.

As shown in the flowchart of the DE algorithm, the estimated parameters at each iteration are evaluated based on the defined cost function. In this work, the described DE algorithm is used to find the listed parameters in Table 2-5. The utilized cost function in this work, which directs the population towards better solutions, is given by:

$$\underset{(\text{params.})}{\mathbf{min}} \left[\sqrt{\frac{\sum_{i=1}^{N}(V_{FC,ex}-V_{FC,mo})^2}{N}} + \sqrt{\frac{\sum_{i=1}^{N}(T_{st,ex}-T_{st,mo})^2}{N}} \right] \tag{2.38}$$

where $V_{FC,ex}$ is the measured output voltage, $V_{FC,mo}$ is the output voltage of the electrochemical model, $T_{st,ex}$ is the measured output temperature, $T_{st,mo}$ is the output temperature of the thermal model, and N is the number of sample data. It should be noted that the upper and lower bounds of the parameters are based on the Table 2 5 . Table 2 6 presents the operating parameters of DE algorithm, which have been used in the optimization problem of this work.

Table 2-6 DE parameters for definition

DE operators	Definition	Value
D	Number of parameters	10
NP	Population number	10
G	Generation number	50
CR	Mutation probability	0.2
F	Mutation scaling factor	[0,2]

2.5.3 Results and discussion

The obtained results regarding the development of the PEMFC emulator, which is composed of a dynamic voltage model and temperature model, are presented in this section. In order to validate the performance of the designed emulator after calibration of the parameters with DE algorithm, the presented current profile in Figure 2.16 has been applied to the emulator and the output voltage and temperature of the emulator have been compared to those of the real PEMFC available on the developed test bench (Figure 2.5). It should be noted that the model calibration of the emulator has been done by using the recorded voltage

and temperature of the real PEMFC corresponded to this current profile. While recording the data, the PEMFC has been operating with a constant duty cycle of 34.

Figure 2.17 compares the emulated voltage and temperature of the developed dynamic model with the real PEMFC. As it is observed in this figure, the model is able to imitate the behavior of a 500-W Horizon PEMFC with a satisfactory precision. The obtained parameters of the model calibration process are shown in Table 2 7 .

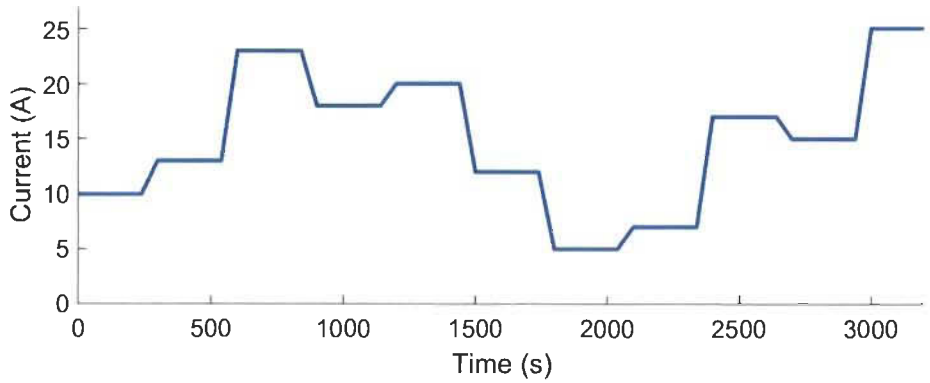

Figure 2.16 Current profile for testing the emulator

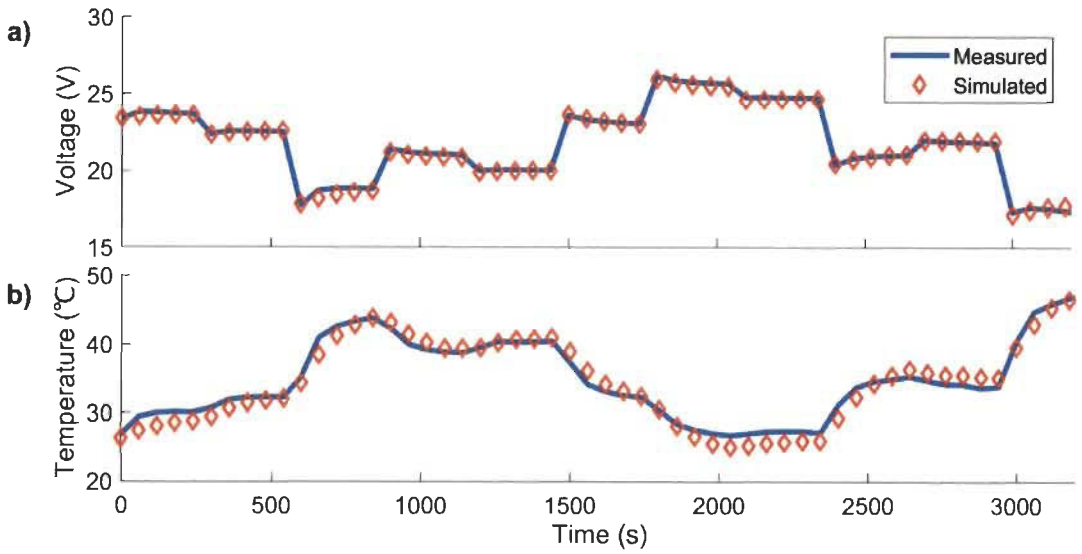

Figure 2.17 Voltage and temperature prediction by the emulator for duty cycle of 34, voltage evolution a), and temperature evolution b)

Table 2-7 Targeted parameters for model calibration

Parameter	Value obtained by DE
ξ_1	-1.505
ξ_2	4.791×10^{-3}
ξ_3	9.182×10^{-5}
ξ_4	-1.892×10^{-5}
c	5.201
B	0.064
ζ_1	8.897×10^{-3}
ζ_2	1.941×10^{-7}
ζ_3	5.765×10^{-6}
α	0.0627

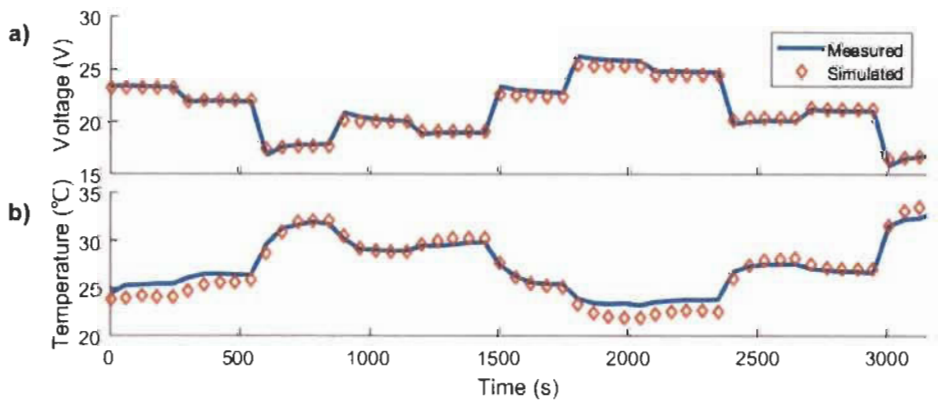

Figure 2.18 Voltage and temperature prediction by the emulator for duty cycle of 100, voltage evolution a), and temperature evolution b)

In order to assess the performance of the calibrated emulator in another operating condition, the same current profile for the duty cycle of 100 have tested. Figure 2.18 represents that the emulator works well in this condition as well. This emulator can be used in the development of the hardware-in-the-loop emulator for a MFCS.

2.6 Synopsis

In this chapter, PEMFC modeling has been explained thoroughly with respect to the aims and objectives of this thesis. The chapter can be divided into two main parts. The first part deals with the development of an online model for the PEMFC, which is necessary for the design of an adaptive energy management strategy. In this regard, a suitable semi-empirical model has been introduced and the process of integrating Kalman filter into the identification of the parameters of this model has been described completely. The main reason for developing an online model is to embrace the performance drifts of the PEMFC due the degradation and operating conditions variations. This part finishes by validating the performance of the online model on a developed test bench in IRH. The second part of this chapter details the development of an emulator for the 500-W Horizon PEMFC. The main reason for developing this emulator is to use it in the MFCS hardware-in-the-loop simulation of this project. This emulator is composed of a dynamic voltage model and a dynamic temperature model. The parameters of the emulator have been calibrated by means of DE. This chapter finishes by validating the performance of the emulator over different operating conditions.

Chapitre 3 - Energy management strategy design

3.1 Introduction

PEMFCs are viewed as one of the most potential sources of power in future transportation applications. They benefit from high energy efficiency and low/zero emissions compared to conventional ICEs and it is mainly attributable to the fact that the electrical energy is generated in them by straight conversion of free energy in fuel without combustion. However, some drawbacks can be counted for powering a vehicle merely by a PEMFC, such as a hefty PEMFC stack power unit due to low power density of this source, lengthy start-up, and slow response to the demanded power. Moreover, in propulsion systems, both of rapid acceleration and low-speed driving result in low-efficiency operating region, as presented in Figure 3.1 . As explained previously, the PEMFC hybridization with a peaking power source is a practical methodology to sort out the discussed problems of a sole PEMFC-powered system. Although hybridization can enhance the system performance to some extent, more attempts are still needed to convince the clients to put their trust in this somehow new emerged technology. One of the proposed methods to improve the reliability and overall performance of a PEMFC hybrid system is to utilize a multi PEMFC stack structure. This structure is an arrangement of several PEMFCs which can work and interact with one another. The MFCS is a totally new system compared to existent conventional hybrid vehicles. It is even more complicated than a typical hybrid PEMFC system and hence an entirely new design control strategy is necessary in this system to exploit its advantages.

The main purpose of this chapter is to propose a novel adaptive EMS for a MFCS. In this respect, this chapter details the utilized structure of the MFCS first. After that, the thorough

explanation of the proposed adaptive strategy is provided along with describing two commonly used EMSs for MFCSs, namely equal distribution and Daisy chain, to be used as a means of comparison. This chapter finishes by explaining the designed hardware-in-the-loop emulator to test the EMSs and discussing the results.

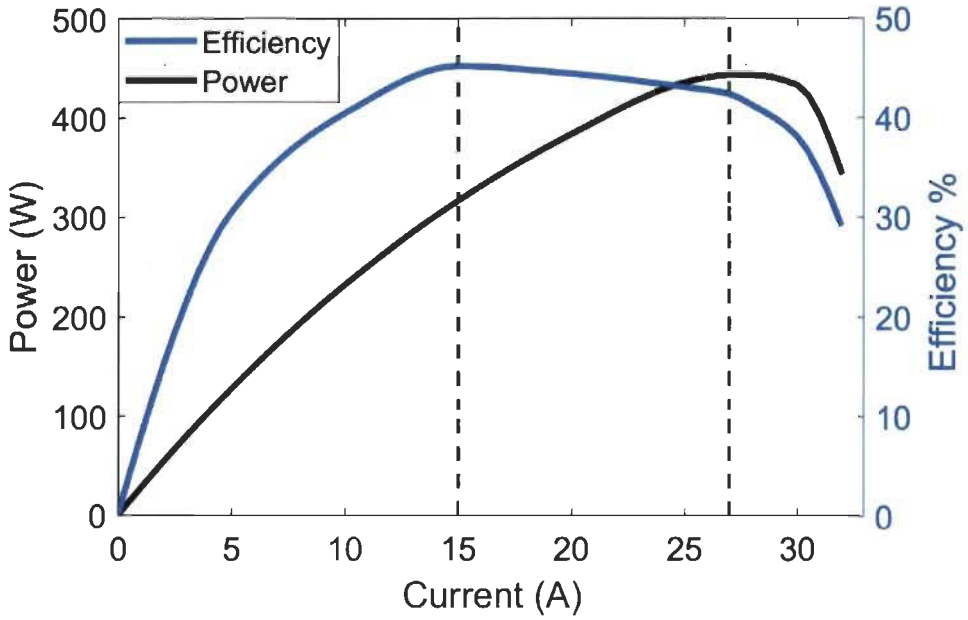

Figure 3.1 Operating characteristics of a PEMFC system from maximum efficiency to maximum power

3.2 Multi-stack fuel cell system configuration

Multi-stack fuel cell systems can be formed in three ways of multiple independent stacks with the shared auxiliary systems, as shown in Figure 3.2 a), modular MFCSs which have independent stacks and auxiliaries, Figure 3.2 b), and segmented fuel cell systems, Figure 3.2 c). The possible architecture designs are determined based on the composition of the system. If the system comprises some PEMFC stacks, different configurations can be used for the electrical, thermal, and other subsystems of the stack. However, in a segmented stack,

the electrical configuration is only flexible and the other subsystems cannot be changed. In this respect, it can be stated that the level of control over the system depends on the type of configuration. In this thesis, the term multi-stack fuel cell system refers to the multiple stacks put together (Figure 3.2 a).

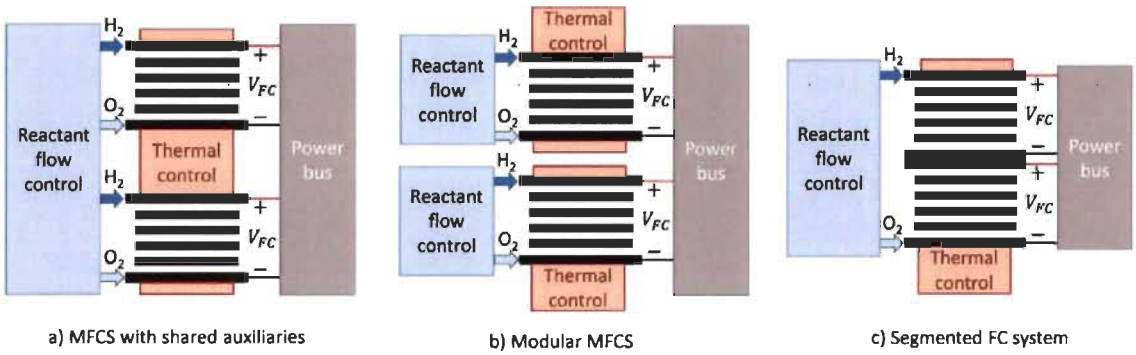

Figure 3.2 multiple FC stack system architectures

A PEMFC is usually connected to the DC bus through a DC-DC converter. The use of converter opens up more possibilities for the configuration. Generally, four configurations of series, parallel, cascade, and series-parallel can be defined for a MFCS, as shown in Figure 3.3 [66, 67]. The simplest and cheapest architecture to implement is the series configuration presented in Figure 3.3 . It can easily reach a higher voltage level by using one low gain power converter that controls the current among all the FCs. The main drawback of this architecture is that if one FC fails, the system stops working. This can be avoided by adding a bypass circuit to isolate that FC, though it can be a critical point during the reconnection process. A parallel connection, as shown in Figure 3.3 , is another way to reach high power level. Connecting power converters to each FC allows the system to have an independent control over the operation conditions of PEMFCs. By using individual converters, it is possible to isolate the degraded PEMFCs and have low-stressed points in the reconnection

process. However, the total cost of the system increases by adopting parallel configuration. Parallel configuration increases the system reliability and fault tolerance, and provides the basis for designing various power distribution strategies [68]. Another configuration, which has been presented in Figure 3.3 c), is Cascade. Indeed, it is one type of series connection, which integrates a low power converter at the output of each FC and connect all the system in series. This architecture allows the individual power control of the FC by means of cheaper regulators. However, the main disadvantage of this configuration is the ripple current present [68]. The last presented configuration is the series-parallel, as shown in Figure 3.3 d). This one combines modularity of parallel and the high voltage level of series connection. The voltage boost is also smaller, which leads to the reduction of the electrical power loss during the elevation voltage process. This configuration is good when the range of operating power is known.

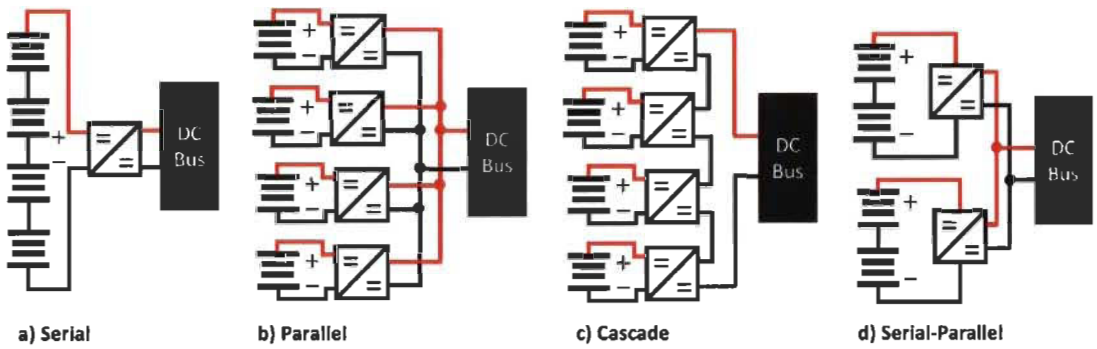

Figure 3.3 Different configurations in a MFCS with DC-DC converters

The utilized configuration in this work is parallel, due to the capability of providing a wide range of requested power, modularity of the system, and various power distribution control possibilities. The utilized MFCS in this work is composed of four PEMFC systems, including their thermal and fuel supply subsystems, and four DC-DC converters. The chosen

configuration leads to more redundancy and modularity, which can enable fault-tolerant operation. Common faults in a PEMFC system are usually due to flooding, drying, and contamination of the system. By having a fault-tolerant operation mode, the MFCS can keep working in case of failure in one of the PEMFCs. The series configuration uses all the FCs at the same time, increasing the degradation. The series-parallel configuration can also provide the same level of redundancy. However, this configuration leads to more complexity in terms of designing an EMS, because the number of modules is reduced. The parallel configuration of the MFCS of this work is presented in Figure 3.4

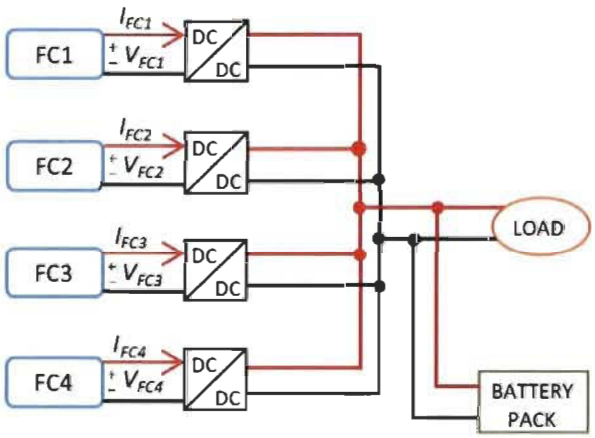

Figure 3.4 Parallel architecture of the utilized MFCS

3.3 Energy management strategy

In a MFCS, the EMS is responsible for distributing the requested power among the power sources with a view to reducing the system degradation as well as the hydrogen consumption. Declining the degradation rate of a MFCS can be achieved by using the minimum possible number of PEMFCs, operating the PEMFCs in their safe zone, and proper management of the battery pack SOC. Diminishing the hydrogen consumption can be reached by enhancing the length of operation in the maximum efficiency region. In this regard an adaptive state

machine based EMS is proposed in this section to fulfill the mentioned objectives in the described MFCS in Figure 3.5 . The performance of this EMS is compared with two common rule-based strategies, namely equal distribution, and Daisy chain, which are explained hereinafter.

- **Adaptive State Machine Based EMS**

In this study, an online EMS, which is called adaptive state machine, is proposed to split the power among the main components, which are four PEMFCs and a battery pack. This strategy has two fundamental operating layers, which is shown in Figure 3.5 . The first layer contains the explained online model in Chapter 2. In fact, it uses a semi-empirical PEMFC model and a Kalman filter to continuously update the maximum power and maximum efficiency of each PEMFC. According to the presented structure in Figure 3.5 , the designed emulator, explained in Chapter 2, acts as the real PEMFC and provides the necessary measurement signals such as voltage, current, and temperature for the online model.

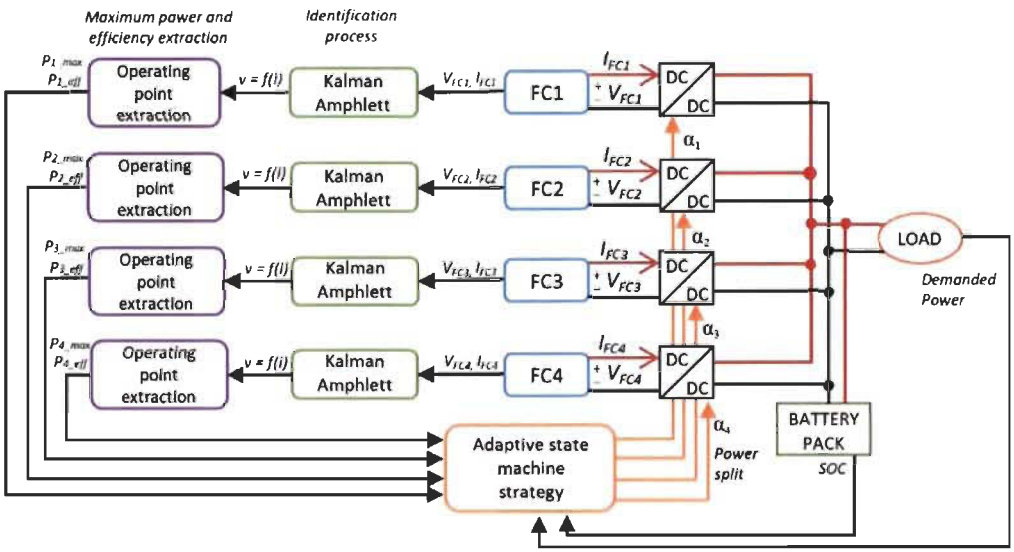

Figure 3.5 MFCS EMS configuration

The second layer of the adaptive state machine strategy distributes the power between the main powertrain components. This layer always attempts to use the minimum number of PEMFCs to meet the requested power. As it can be seen in Figure 3.5 , this layer has four inputs, which are the updated maximum power and maximum efficiency, battery SOC, and the requested power. The updated maximum power and efficiency points are firstly used to reconfigure the order of using the PEMFCs. In fact, the PEMFCs are always put in a descending order from young to old. The age of each fuel cell is decided based on its current maximum efficiency and power, which means the more power and efficiency, the younger. It should be noted that in this manuscript, the term ''young fuel cell'' refers to the PEMFC with the highest power level and the term ''old fuel cell'' refers to the PEMFC with the lowest power level. The difference in the level of the PEMFCs power can be owing to the aging phenomena and operation time or any malfunctions in the system. The second practical usage of these updated points is that the strategy employs each PEMFC in a way to be between ME and MP range, which is a safe and efficient region. This is mainly due to the fact that by remaining in this region, fuel cell does not operate in activation, which is near open circuit voltage, and concentration zones. Working in both of these zones expedites the aging phenomenon. The other two inputs, which are battery SOC and demanded power, are used to allocate some portions of the requested power to the components. Figure 3.6 presents the configuration of the proposed adaptive state machine EMS. In brief, this strategy first imposes the same requested power to all the FCs in order to identify their characteristics and analyzes the inputs. Subsequently, it sorts out the PEMFCs in terms of their maximum power by utilizing an active table. Finally, it supplies the demanded power in a particular sequence in which the PEMFC with the best performance is first used up to its maximum power. If the demanded power exceeds the maximum power of the first PEMFC, the second PEMFC in

the active table is turned on only if this remnant is inside its efficiency zone. Otherwise the battery supplies this power and this logic is applied to the rest of the PEMFCs. One of the advantages of the proposed strategy is that it degrades all the PEMFCs equally even if they have different aging rates.

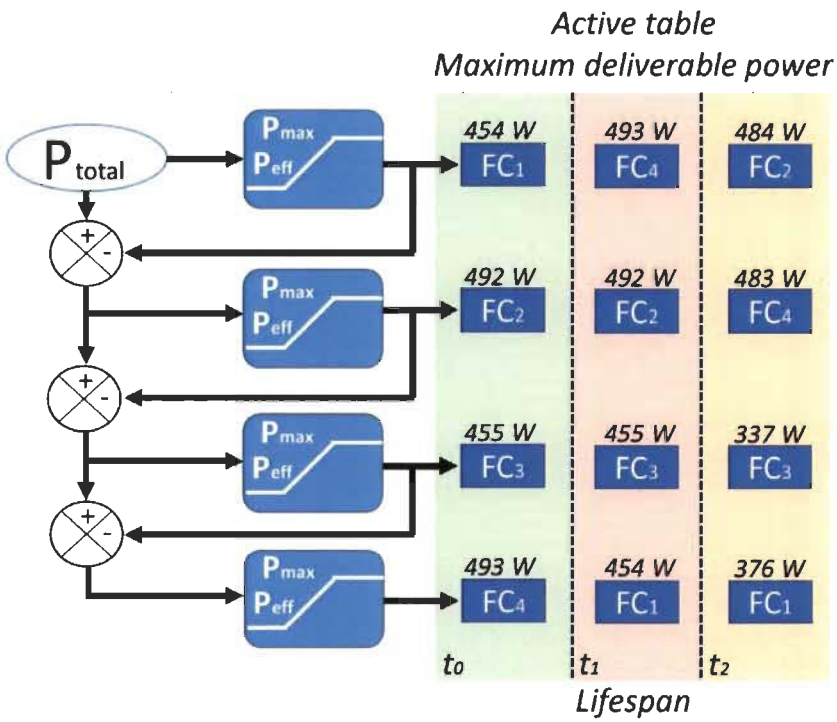

Figure 3.6 Adaptive state machine EMS

- **Equal distribution strategy**

Equal distribution strategy is based on dividing the requested power equally as the number of available PEMFCs. This strategy uses the requested power (P_{req}) as the only input signal, as described below.

$$P_{FC_i} = {}^{P_{req}}/_{N} \tag{3.1}$$

Where P_{FCi} is the requested power from the FC_i, determined by (3.1), and N is the number of available fuel cells. In this strategy, all the PEMFCs have the same demanding power in

spite of having different electrical capabilities in terms of supplying power and electrical response. It is worth mentioning that the utilized PEMFCs in this strategy are aged at the same rate regardless of their initial degradation level.

- **Daisy chain strategy**

In a parallel configuration, Daisy Chain strategy utilizes the minimum number of PEMFCs to supply the requested power in a sequential order. This strategy employs only the first PEMFC until it reaches its MP. The next PEMFC is activated afterwards to supply the remaining requested power. This strategy has been tested in a MFCS in [17] and presented a better performance in low power demand compared to equal distribution method. On the other hand, equal distribution method presents a better response when the demanded power is high. Daisy Chain strategy considers the total demanded power from the system and the maximum power of each PEMFC as inputs. The main disadvantage of this strategy is that it uses the FCs in a fixed order, causing the most part of degradation on the first FC. Therefore, the FCs are sorting randomly each 30 minutes.

3.4 Results and discussion

The obtained results from implementing the introduced EMSs are comprehensibly discussed in this section. In order to investigate carefully the performance of the proposed EMS, three different scenarios have been designed. In the first scenario, a ramp power profile has been used to clearly show the difference between the distribution of the power between different sources by the three strategies. The second scenario deals with the performance evaluation of the EMSs while using a real driving profile from Nemo vehicle. Finally, the last scenario has been designed by employing a very long random step power profile to assess

the degradation rate of the MFCS under different EMSs. It should be noted that the minimum requested power that equal distribution and Daisy chain strategies impose to the system is limited to 80 W per fuel cell, which has been recommended as the minimum drawn power by the manufacturer, in order to avoid unnecessary turn-on cycles which could interfere with the real performance of the strategies. This limitation means that while the requested power from each PEMFC is less than 80 W, the battery pack will supply it. Regarding the power limitations of the proposed adaptive state machine EMS, the PEMFCs work between the maximum efficiency and maximum power points which are defined by the online modeling process. Another worth mentioning point is that in scenarios 1 and 2, FC4 is the real PEMFC, and FC1 to FC3 are the emulators. However, in scenario 3, which is a very long test and the usage of a real PEMFC is highly time-consuming, all of FC1 to FC4 are emulators.

3.4.1 Scenario 1:

Figure 3.7 shows the utilized demanded power profile in this scenario. As it is seen in this figure, this profile is a ramp-up power profile, which makes the functionality of different EMSs clear in terms of power distribution. It also indicates the way that the proposed strategy of this work reconfigures the order of using the PEMFCs. The presented power profile in Figure 3.7 has been applied to the MFCS for two different initial conditions in terms of age of each PEMFC to illustrate the change of the order for different conditions. The initial ages for performing this test are presented in Table 3 1 . This age is used as the input of the degradation function to determine the characteristics of the system with respect to the aging phenomena.

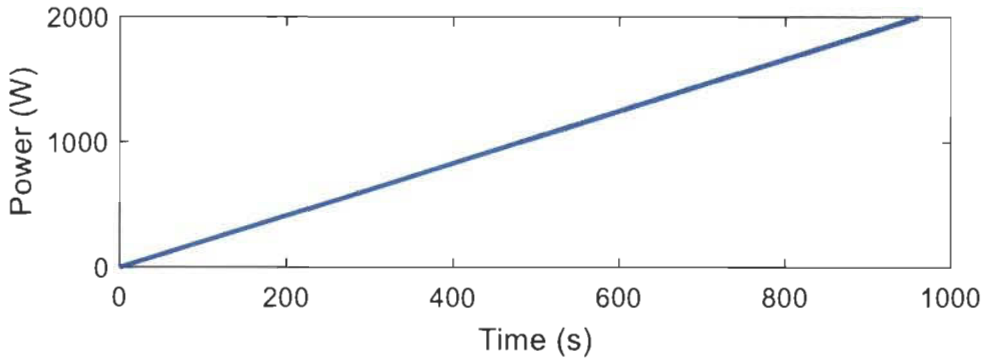

Figure 3.7 Ramp profile

Table 3-1 Initial conditions for performing the ramp profile test

PEMFC system	Condition 1: Age (h)	Condition 2: Age (h)
FC1	1000	1000
FC2	4000	3000
FC3	1000	2000
FC4	4000	4000

Figure 3.8 shows the supplied power by the four PEMFCs and the battery for all the three strategies. According to Figure 3.8 a), Equal distribution strategy uses the battery in the beginning to supply the requested power up to 320 W, which means 80 W per PEMFC. Then the PEMFCs equally supply the requested power from almost 150 s to around 700 s. From 700 s onwards, since the level of the requested power is very high, FC4 and FC2, which are more degraded than the others, work in their maximum power and FC1 and FC3 converge to their maximum limit to meet the demanded power. The battery pack also helps the PEMFCs in this respect. With regard to the Daisy chain strategy, Figure 3.8 b), it can be observed that this strategy turns on FC4 when the requested power exceeds 80 W and uses this FC until its

maximum power. Then, it turns on more FCs as the requested power increases. One important aspect that should be pointed out here is that since this strategy is not aware of the current maximum achievable power of the PEMFCs, it has used the more degraded PEMFCs more than other two PEMFCs, which can lead to less efficiency of the system. Furthermore, the supplied power by the battery in Figure 3.8 b) indicates that when the degraded PEMFCs reach their maximum power, which is 400 W in this case, the strategy assumes that the rated power is 500 W. As a result, battery supplies this difference between the actual maximum power of the FC and its initial rated power, and when the limiting power for activating the next FC is passed, it will be turned on. It should be reminded that the PEMFCs order is changed randomly from time to time in Daisy chain strategy. Concerning the proposed adaptive state machine EMS, Figure 3.8 c), it can be seen that in the beginning, a power level is applied to all the PEMFCs to identify the real maximum power and efficiency of all the FCs by means of the previously explained online modeling procedure. During this short period of time, the battery supplies the requested power. From 50 s onward, the battery meets the demanded power up to the point that the requested power reaches the maximum efficiency level of the FC1. The strategy keeps using the FC1 up to its identified maximum power level. Then the next FCs are activated by respecting the same rules and regulations to satisfy the request. The point that needs to be highlighted is that in the proposed strategy, FC1 and FC3, which are in better state of health according to the defined conditions in Table 3 1 , are used more than the other two FCs. This choice has been made based on the performed identification process in the beginning and it can result in higher efficiency of the system, which will be explored more hereinafter.

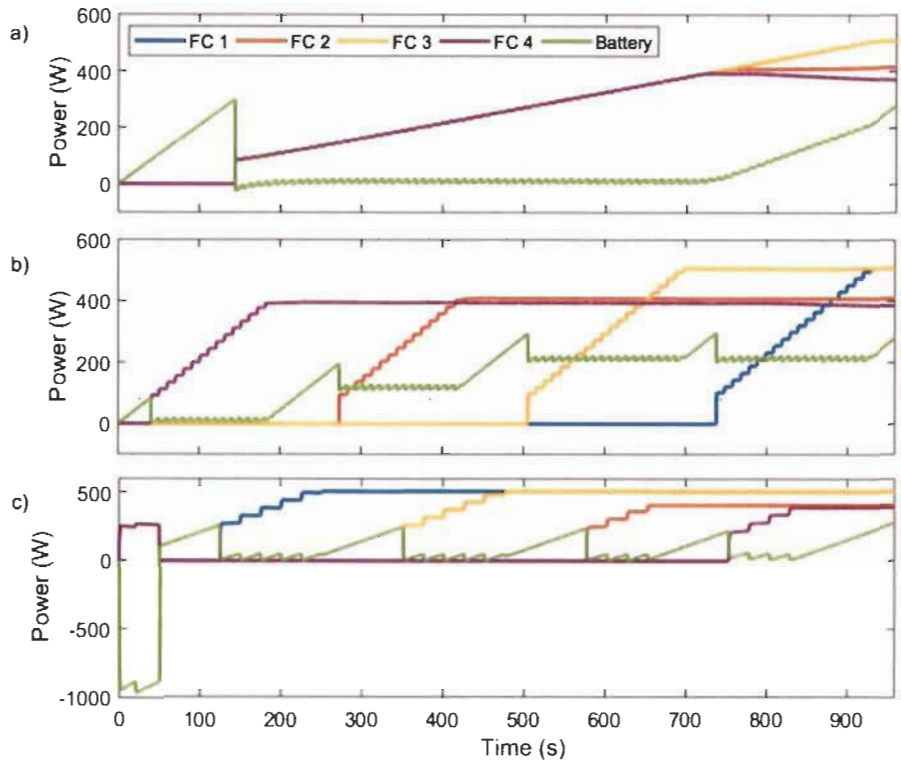

Figure 3.8 Power split for Condition 1, a) Equal distribution, b) Daisy Chain, and c) Adaptive State Machine

Figure 3.9 represents the distribution of the power by the three algorithms for Condition 2, specified in Table 3 1 . As it can be seen in this figure, the same principle as Condition 1 has been followed by the algorithms in terms of power sharing. However, the conditions of the PEMFCs are different, and accordingly the proposed adaptive state machine EMS has reconfigured the order of the PEMFCs from the youngest to the most degraded one (FC1, FC3, FC2, and FC4). These two tests have been presented to show the functionality of the proposed EMS regarding the powering sharing. Figure 3.10 indicates the hydrogen consumption for the both discussed conditions. According to this figure, Daisy Chain strategy has the highest hydrogen consumption due to the fact that it has used the more degraded PEMFCs for a longer period of time than the other strategies. Equal distribution strategy

shows a better fuel economy than the Daisy chain and it can be attributed to its better performance in low current level conditions. The proposed EMS has the best fuel economy, which is the result of the reconfiguration of the order of the PEMFCs as well as keeping the PEMFCs operating conditions within the safe zone between maximum power and efficiency points. It should be noted that in order to compare the achieved fuel consumption of the strategies, the initial battery SOC is 70% and it is expected that they finish in the same level. The hydrogen consumption, which is needed to recharge the battery pack to reach the same level as the its initial state has been calculated and added to consumption of each strategy.

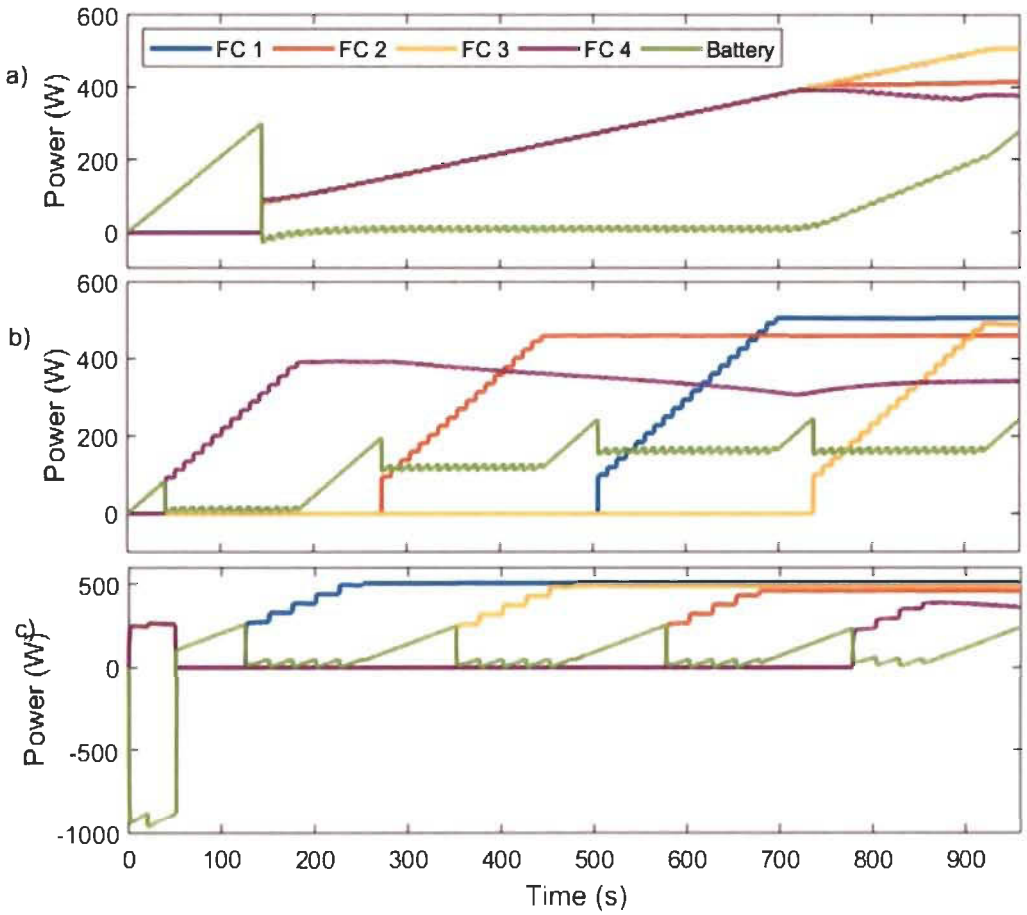

Figure 3.9 Power split for Condition 2, a) Equal distribution, b) Daisy Chain, c) Adaptive State Machine

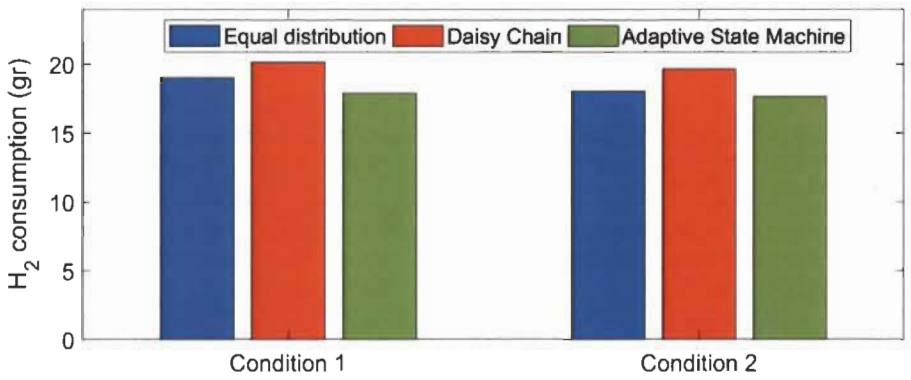

Figure 3.10 Hydrogen consumption for the two conditions using the ramp profile

3.4.2 Scenario 2:

In this scenario, Highway Fuel Economy Test Cycle (HWFET) developed by the US EPA has been used to assess the power distribution of the EMSs in real condition. This driving cycle and its corresponded requested power profile are shown in Figure 3.11 . The power profile has been extracted by using the Nemo vehicle drive train information and equation (2.1).

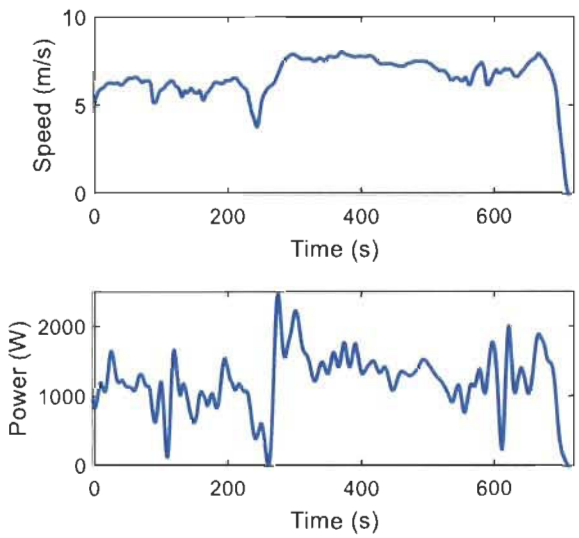

Figure 3.11 HWFET profile, a) Speed profile, b) Requested power from Nemo drive train.

Figure 3.12 shows the power split achieved by the three strategies for the introduced HWFET profile. As it can be seen in this figure, in all the cases, the battery supplies the power peaks. Equal distribution and Daisy Chain strategies try to make the FCs work between low to high power region. On the other hand, the proposed strategy attempts to keep the FCs in a constant state for a longer time, which leads to reducing the number of PEMFC on/off cycles compared to Daisy Chain. Table 3 2 compares the fuel consumption achieved by different strategies. In order to have a fair comparison, the initial and final battery SOC is set to 70 %, similar to Scenario 1.

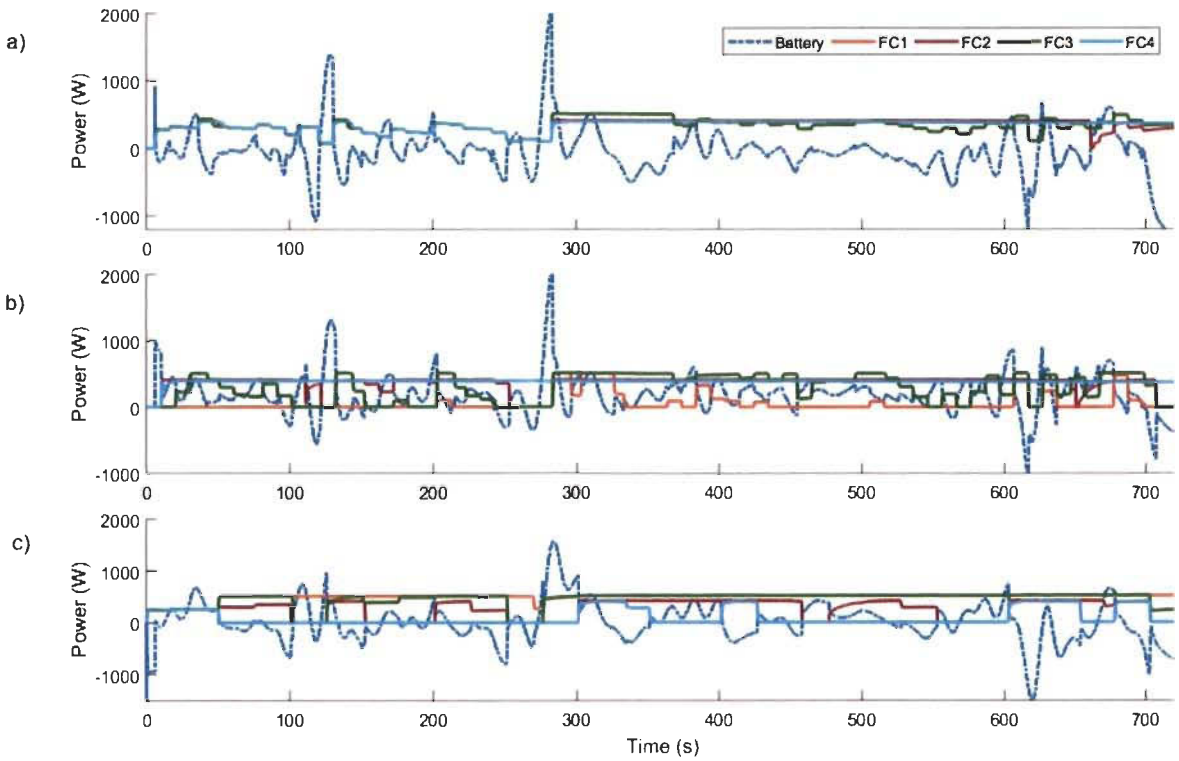

Figure 3.12 Power split for the three strategies, a) Equal distribution, b) Daisy Chain, and c) Adaptive State Machine

Table 3-2 Hydrogen consumption for the studied strategies and percentage reduction of the proposed strategy

Strategy	H2 consumption (gr)	% Reduction
Equal distribution	16,09	8.6 %
Daisy Chain	16,84	12.7%
Adaptive State Machine	14,69	-

3.4.3 Scenario 3:

In this last scenario, a random step profile of 25 minutes, as shown in Figure 3.13, has been repeated for 300 hours. It is worth noting that fuel cell systems of the same model can show various degradation behavior, and it can be attributable to several reasons such as their fabrication process and working conditions. In this regard, during this long test, different ageing rates have been applied to the fuel cells to evaluate the performance of the strategies regarding coping with degradation management. As explained earlier, one of the main capabilities of the proposed EMS of this work is to make the PEMFC systems' degradation equal and the main purpose of designing this scenario is to illustrate this advantage. Table 3-3 shows the utilized degradation rate for each PEMFC throughout this scenario. Each indicated degradation rate acts as an accelerated factor, which will be multiplied by (2.35).

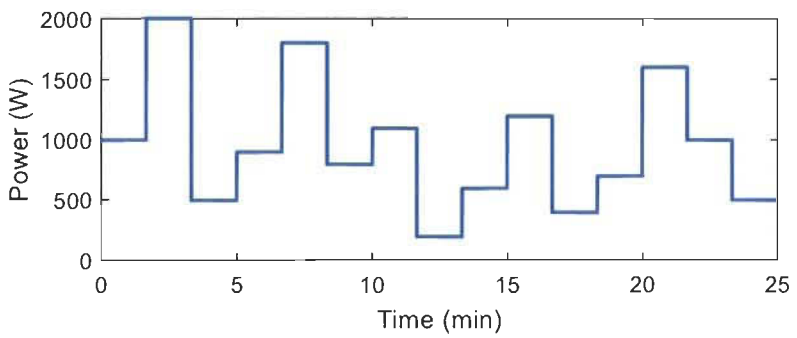

Figure 3.13 Random step power profile unit

Table 3-3 Degradation rate

FC number	Degradation rate
FC1	5.7
FC2	3.7
FC3	4.3
FC4	3.2

Figure 3.14 demonstrates the maximum power evolution of each fuel cell system which is affected by the specified degradation rate in Table 3 3 . This maximum power trend is a good measure to compare the performance of the EMSs through the time. As it is clear in Figure 3.14 , the PEMFCs get degraded by different rates in case of equal distribution and Daisy Chain strategies. However, the proposed Adaptive state machine EMS manages to keep the PEMFCs with almost the same degradation rate by reconfiguring their order from time to time. The maximum observable difference in the power of the PEMFCs is 10 W. It should be noted that keeping the FCs within a similar degradation rate can lower the hydrogen consumption, increase the system life time, and extend the replacement time of each PEMFC. Figure 3.15 clarifies the operation time of each PEMFC during the long test. As expected, the proposed EMS uses the more degraded PEMFCs less (FC1:135.6 h and FC3:148.1 h) than the other two PEMFCs (FC2:189.2 h and FC4:177.7 h). It is also observed that the equal distribution strategy utilizes all the PEMFCs for 280.7 h, and Daisy Chain strategy does not respect the state of the health of the PEMFCs while using them (FC1: 178.7 h, FC2: 189.2 h, FC3: 199.5 h, and FC4: 175.1). Table 3 4 presents the hydrogen consumption of each EMS for the performed test and the percentage decrease of hydrogen consumption compare to the proposed strategy.

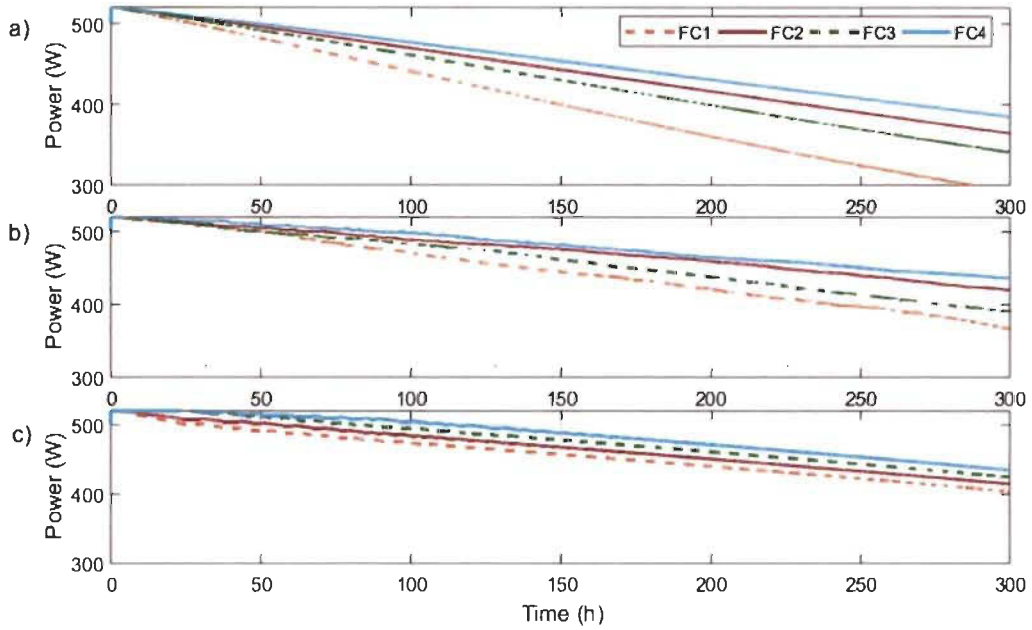

Figure 3.14 Maximum power evolution during the 300-h test. a) Equal distribution, b) Daisy Chain, c) Adaptive State Machine

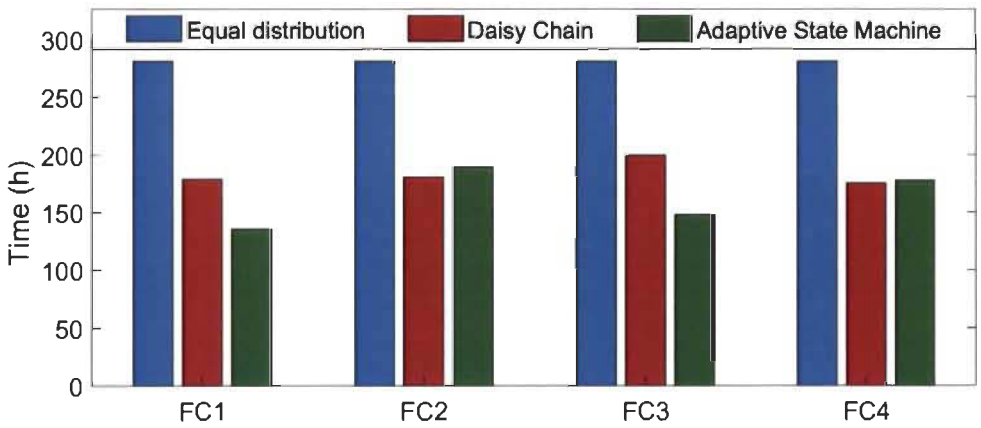

Figure 3.15 Operation time of each PEMFC during the 300-h test

Table 3-4 Hydrogen consumption comparison for the 300-h test and percentage reduction of the proposed strategy

Strategy	H2 consumption (l)	% Reduction
Equal distribution	63494,8	26.5 %
Daisy Chain	55223,4	15.4 %
Adaptive State Machine	46697,3	-

One of the main factors which help to reduce the hydrogen consummation is to avoid using the PEMFCs in low power level regions and supplying it by the battery. In fact, battery plays a dual role in this hybrid system by supplying the low-level requested power as well as absorbing the power peaks. It is important to highlight that the SOC of the battery has been recommended to be more than 50 % in order to extend its lifetime. Figure 3.16 shows the battery SOC for the 300-hours test. At the end of the test, the battery has been fully charged by the PEMFCs to have a fair comparison.

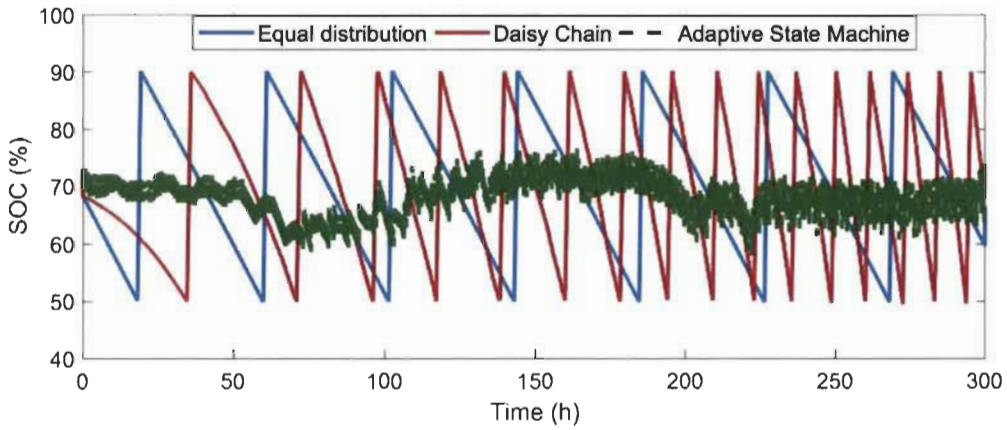

Figure 3.16 Battery SOC evolution during the 300-h test.

Chapitre 4 - Conclusion

This work addresses the design of an adaptive EMS for a multi-source system, which comprises four PEMFCs and a battery pack, with the aim of reducing the hydrogen consumption as well as enhancing the lifetime of the system. The proposed strategy, which is called adaptive state machine, takes into consideration four inputs, namely battery state of charge, requested power from the system, maximum power and maximum efficiency points of the PEMFCs, to conduct the power sharing among the sources. The maximum power and efficiency points of the PEMFCs are continuously determined by using an online model composed of a Kalman filter integrated into a PEMFC semi-empirical model for each PEMFC. The updated operating points are used by the strategy to decide on the order of the PEMFCs from young (the PEMFC with the highest power level) to old (the PEMFC with the lowest power level). The strategy uses the minimum possible number of the PEMFCs to meet the requested power and the updated maximum power determines the limit which can be asked from each PEMFC. Three scenarios of ramp power profile, real driving profile, and a long random step profile have been designed to evaluate the performance of the proposed strategy. Moreover, two commonly used power sharing strategies of equal distribution and Daisy chain in MFCSs have been tested with the mentioned scenarios to make a comparison with the suggested adaptive state strategy. The final results of this work indicated the superior performance of the proposed EMS in terms of fuel consumption and lifetime. In fact, for a performed 300-hour test, which is quite a long test, up to 25% fuel consumption reduction has been achieved by the proposed strategy compared to the commonly used EMSs for MFCSs.

References

[1] J. Larminie, A. Dicks, J. Larminie, and A. Dicks, "Introduction," in *Fuel Cell Systems Explained*, ed: John Wiley & Sons, Ltd,. 2013, pp. 1-24.

[2] H. S. Das, C. W. Tan, and A. H. M. Yatim, "Fuel cell hybrid electric vehicles: A review on power conditioning units and topologies," *Renewable and Sustainable Energy Reviews,* vol. 76, pp. 268-291, 2017/09/01/ 2017.

[3] A. F. Ambrose, A. Q. Al-Amin, R. Rasiah, R. Saidur, and N. Amin, "Prospects for introducing hydrogen fuel cell vehicles in Malaysia," *International Journal of Hydrogen Energy,* vol. 42, pp. 9125-9134, 2017/04/06/ 2017.

[4] N. Marx, D. Hissel, F. Gustin, L. Boulon, and K. Agbossou, "On the sizing and energy management of an hybrid multistack fuel cell – Battery system for automotive applications," *International Journal of Hydrogen Energy,* vol. 42, pp. 1518-1526, 2017.

[5] N. Marx, L. Boulon, F. Gustin, D. Hissel, and K. Agbossou, "A review of multi-stack and modular fuel cell systems: Interests, application areas and on-going research activities," *International Journal of Hydrogen Energy,* vol. 39, pp. 12101-12111, 2014.

[6] G. J. Offer, D. Howey, M. Contestabile, R. Clague, and N. P. Brandon, "Comparative analysis of battery electric, hydrogen fuel cell and hybrid vehicles in a future sustainable road transport system," *Energy Policy,* vol. 38, pp. 24-29, 2010/01/01/ 2010.

[7] N. Marx, J. Cardozo, L. Boulon, F. Gustin, D. Hissel, and K. Agbossou, "Comparison of the Series and Parallel Architectures for Hybrid Multi-Stack Fuel Cell - Battery Systems," in *2015 IEEE Vehicle Power and Propulsion Conference (VPPC)*, 2015, pp. 1-6.

[8] R. Long, Z. Yin, L. Zhang, Q. Chen, and S. Quan, "Design of power allocation strategy and passivity based controller for multiple module fuel cell hybrid power system," in *2017 29th Chinese Control And Decision Conference (CCDC)*, 2017, pp. 4944-4948.

[9] N. Sulaiman, M. A. Hannan, A. Mohamed, E. H. Majlan, and W. R. Wan Daud, "A review on energy management system for fuel cell hybrid electric vehicle: Issues and challenges," *Renewable and Sustainable Energy Reviews,* vol. 52, pp. 802-814, 2015.

[10] X. Hu, N. Murgovski, L. M. Johannesson, and B. Egardt, "Optimal Dimensioning and Power Management of a Fuel Cell/Battery Hybrid Bus via Convex Programming," *IEEE/ASME Transactions on Mechatronics,* vol. 20, pp. 457-468, 2015.

[11] K. Simmons, Y. Guezennec, and S. Onori, "Modeling and energy management control design for a fuel cell hybrid passenger bus," *Journal of Power Sources,* vol. 246, pp. 736-746, 2014/01/15/ 2014.

[12] C. Min and G. A. Rincon-Mora, "Accurate electrical battery model capable of predicting runtime and I-V performance," *IEEE Transactions on Energy Conversion,* vol. 21, pp. 504-511, 2006.

[13] B. M. Institute, "Manufacturing cost analysis of 10 kW and 25 kW direct hydrogen Polymer Electrolyte Membrane (PEM) fuel cell for material handling applications," U.S. Department of Energy 2013.

[14] A. Panday and H. O. Bansal, "A Review of Optimal Energy Management Strategies for Hybrid Electric Vehicle," *International Journal of Vehicular Technology,* vol. 2014, p. 19, 2014.

[15] M. K. Dayeni, A. Macias, C. Depature, L. Boulon, S. Kelouwani, and H. Chaoui, "Real-Time Fuzzy Logic Strategy Scheme for Energetic Macroscopic Representation of a Fuel Cell/Battery Vehicle," in *2017 IEEE Vehicle Power and Propulsion Conference (VPPC)*, 2017, pp. 1-6.

[16] M. Becherif, F. Claude, T. Hervier, and L. Boulon, "Multi-stack Fuel Cells Powering a Vehicle," *Energy Procedia,* vol. 74, pp. 308-319, 2015.

[17] D. C. T. Cardenas, N. Marx, L. Boulon, F. Gustin, and D. Hissel, "Degraded Mode Operation of Multi-Stack Fuel Cell Systems," in *2014 IEEE Vehicle Power and Propulsion Conference (VPPC)*, 2014, pp. 1-6.

[18] J. E. Garcia, D. F. Herrera, L. Boulon, P. Sicard, and A. Hernandez, "Power sharing for efficiency optimisation into a multi fuel cell system," in *2014 IEEE 23rd International Symposium on Industrial Electronics (ISIE)*, 2014, pp. 218-223.

[19] N. Marx, D. C. T. Cárdenas, L. Boulon, F. Gustin, and D. Hissel, "Degraded mode operation of multi-stack fuel cell systems," *IET Electrical Systems in Transportation,* vol. 6, pp. 3-11, 2016.

[20] M. Kandi Dayeni and M. Soleymani, "Intelligent energy management of a fuel cell vehicle based on traffic condition recognition," *Clean Technologies and Environmental Policy,* vol. 18, pp. 1945-1960, 2016.

[21] M. Kandi-D, M. Soleymani, and A. A. Ghadimi, "Designing an Optimal Fuzzy Controller for a Fuel Cell Vehicle Considering Driving Patterns," *Scientia Iranica,* vol. 23, pp. 218-227, 2016.

[22] Q. Li, H. Yang, Y. Han, M. Li, and W. Chen, "A state machine strategy based on droop control for an energy management system of PEMFC-battery-supercapacitor hybrid tramway," *International Journal of Hydrogen Energy,* vol. 41, pp. 16148-16159, 2016.

[23] F. Peng, Y. Zhao, X. Li, Z. Liu, W. Chen, Y. Liu, *et al.*, "Development of master-slave energy management strategy based on fuzzy logic hysteresis state machine and differential power processing compensation for a PEMFC-LIB-SC hybrid tramway," *Applied Energy,* vol. 206, pp. 346-363, 2017.

[24] T. Wang, Q. Li, W. Chen, and T. Liu, "Application of energy management strategy based on state machine in fuel cell hybrid power system," in *2017 IEEE*

Transportation Electrification Conference and Expo, Asia-Pacific (ITEC Asia-Pacific), 2017, pp. 1-5.

[25] R. Álvarez Fernández, S. Corbera Caraballo, F. Beltrán Cilleruelo, and J. A. Lozano, "Fuel optimization strategy for hydrogen fuel cell range extender vehicles applying genetic algorithms," *Renewable and Sustainable Energy Reviews,* vol. 81, pp. 655-668, 2018.

[26] B. Geng, J. K. Mills, and D. Sun, "Combined power management/design optimization for a fuel cell/battery plug-in hybrid electric vehicle using multi-objective particle swarm optimization," *International Journal of Automotive Technology,* vol. 15, pp. 645-654, June 01 2014.

[27] F. d. C. Lopes, S. Kelouwani, L. Boulon, K. Agbossou, N. Marx, and K. Ettihir, "Neural network modeling strategy applied to a multi-stack PEM fuel cell system," in *2016 IEEE Transportation Electrification Conference and Expo (ITEC)*, 2016, pp. 1-7.

[28] Z. Hu, J. Li, L. Xu, Z. Song, C. Fang, M. Ouyang, *et al.*, "Multi-objective energy management optimization and parameter sizing for proton exchange membrane hybrid fuel cell vehicles," *Energy Conversion and Management,* vol. 129, pp. 108-121, 2016.

[29] S. Caux, Y. Gaoua, and P. Lopez, "A combinatorial optimisation approach to energy management strategy for a hybrid fuel cell vehicle," *Energy,* vol. 133, pp. 219-230, 2017.

[30] N. Bizon, "Real-time optimization strategy for fuel cell hybrid power sources with load-following control of the fuel or air flow," *Energy Conversion and Management,* vol. 157, pp. 13-27, 2018.

[31] N. Herr, J.-M. Nicod, C. Varnier, L. Jardin, A. Sorrentino, D. Hissel, *et al.*, "Decision process to manage useful life of multi-stacks fuel cell systems under service constraint," *Renewable Energy,* vol. 105, pp. 590-600, 2017.

[32] D. Li, Y. Yu, Q. Jin, and Z. Gao, "Maximum power efficiency operation and generalized predictive control of PEM (proton exchange membrane) fuel cell," *Energy,* vol. 68, pp. 210-217, 2014.

[33] C. A. Ramos-Paja, G. Spagnuolo, G. Petrone, and E. Mamarelis, "A perturbation strategy for fuel consumption minimization in polymer electrolyte membrane fuel cells: Analysis, Design and FPGA implementation," *Applied Energy,* vol. 119, pp. 21-32, 2014.

[34] D. Zhou, A. Ravey, A. Al-Durra, and F. Gao, "A comparative study of extremum seeking methods applied to online energy management strategy of fuel cell hybrid electric vehicles," *Energy Conversion and Management,* vol. 151, pp. 778-790, 2017.

[35] M. Kandidayeni, A. Macias, A. A. Amamou, L. Boulon, S. Kelouwani, and H. Chaoui, "Overview and benchmark analysis of fuel cell parameters estimation for energy management purposes," *Journal of Power Sources,* vol. 380, pp. 92-104, 2018.

[36] K. Ettihir, L. Boulon, and K. Agbossou, "Optimization-based energy management strategy for a fuel cell/battery hybrid power system," *Applied Energy,* vol. 163, pp. 142-153, 2016.

[37] K. Ettihir, M. Higuita Cano, L. Boulon, and K. Agbossou, "Design of an adaptive EMS for fuel cell vehicles," *International Journal of Hydrogen Energy,* vol. 42, pp. 1481-1489, 2017.

[38] K. Ettihir, L. Boulon, and K. Agbossou, "Energy management strategy for a fuel cell hybrid vehicle based on maximum efficiency and maximum power identification," *IET Electrical Systems in Transportation,* vol. 6, pp. 261-268, 2016.

[39] K. Ettihir, L. Boulon, M. Becherif, K. Agbossou, and H. S. Ramadan, "Online identification of semi-empirical model parameters for PEMFCs," *International Journal of Hydrogen Energy,* vol. 39, pp. 21165-21176, 2014.

[40] C. Li, "The optimization of hydrogen consumption based on the controlling of charging circuit in Nemo hybrid electric vehicle," Master Degree, Génie électrique, Université du Québec à Trois-Rivières, 2015.

[41] L. Lu, X. Han, J. Li, J. Hua, and M. Ouyang, "A review on the key issues for lithium-ion battery management in electric vehicles," *Journal of Power Sources,* vol. 226, pp. 272-288, 2013.

[42] K. Thirugnanam, P. E. R. J. T, M. Singh, and P. Kumar, "Mathematical Modeling of Li-Ion Battery Using Genetic Algorithm Approach for V2G Applications," *IEEE Transactions on Energy Conversion,* vol. 29, pp. 332-343, 2014.

[43] U. BATTERY. (2013). *Datasheet Deep Cycle 8 -Volt.*

[44] R. F. Mann, J. C. Amphlett, M. A. I. Hooper, H. M. Jensen, B. A. Peppley, and P. R. Roberge, "Development and application of a generalised steady-state electrochemical model for a PEM fuel cell," *Journal of Power Sources,* vol. 86, pp. 173-180, 2000/03/01/ 2000.

[45] A. Saadi, M. Becherif, A. Aboubou, and M. Y. Ayad, "Comparison of proton exchange membrane fuel cell static models," *Renewable Energy,* vol. 56, pp. 64-71, 2013.

[46] G. Squadrito, G. Maggio, E. Passalacqua, F. Lufrano, and A. Patti, "An empirical equation for polymer electrolyte fuel cell (PEFC) behaviour," *Journal of Applied Electrochemistry,* vol. 29, pp. 1449-1455, December 01 1999.

[47] M. Kandidayeni, A. Macias, A. A. Amamou, L. Boulon, and S. Kelouwani, "Comparative Analysis of Two Online Identification Algorithms in a Fuel Cell System," *Fuel Cells,* vol. 18, pp. 347-358, 2018.

[48] K. R. Cooper and M. Smith, "Electrical test methods for on-line fuel cell ohmic resistance measurement," *Journal of Power Sources,* vol. 160, pp. 1088-1095, 2006.

[49] T. Mennola, M. Mikkola, M. Noponen, T. Hottinen, and P. Lund, "Measurement of ohmic voltage losses in individual cells of a PEMFC stack," *Journal of Power Sources,* vol. 112, pp. 261-272, 2002/10/24/ 2002.

[50] C. Depature, S. Jemei, L. Boulon, A. Bouscayrol, N. Marx, S. Morando, *et al.*, "IEEE VTS Motor Vehicles Challenge 2017 - Energy Management of a Fuel Cell/Battery Vehicle," in *2016 IEEE Vehicle Power and Propulsion Conference (VPPC)*, 2016, pp. 1-6.

[51] M. Ali, M. A. El-Hameed, and M. A. Farahat, "Effective parameters' identification for polymer electrolyte membrane fuel cell models using grey wolf optimizer," *Renewable Energy,* vol. 111, pp. 455-462, 2017.

[52] A. A. El-Fergany, "Extracting optimal parameters of PEM fuel cells using Salp Swarm Optimizer," *Renewable Energy,* vol. 119, pp. 641-648, 2018.

[53] K. Priya, T. Sudhakar Babu, K. Balasubramanian, K. Sathish Kumar, and N. Rajasekar, "A novel approach for fuel cell parameter estimation using simple Genetic Algorithm," *Sustainable Energy Technologies and Assessments,* vol. 12, pp. 46-52, 2015.

[54] N. Rajasekar, B. Jacob, K. Balasubramanian, K. Priya, K. Sangeetha, and T. Sudhakar Babu, "Comparative study of PEM fuel cell parameter extraction using Genetic Algorithm," *Ain Shams Engineering Journal,* vol. 6, pp. 1187-1194, 2015.

[55] V. Boscaino, R. Miceli, and G. Capponi, "MATLAB-based simulator of a 5 kW fuel cell for power electronics design," *International Journal of Hydrogen Energy,* vol. 38, pp. 7924-7934, 2013.

[56] K. J. Runtz and M. D. Lyster, "Fuel cell equivalent circuit models for passive mode testing and dynamic mode design," in *Canadian Conference on Electrical and Computer Engineering, 2005.*, 2005, pp. 794-797.

[57] K. Haraldsson and K. Wipke, "Evaluating PEM fuel cell system models," *Journal of Power Sources,* vol. 126, pp. 88-97, 2004.

[58] L. Je and A. Dicks, *Fuel Cell System Explained*, 2013.

[59] C. Restrepo, T. Konjedic, A. Garces, J. Calvente, and R. Giral, "Identification of a Proton-Exchange Membrane Fuel Cell's Model Parameters by Means of an Evolution Strategy," *IEEE Transactions on Industrial Informatics,* vol. 11, pp. 548-559, 2015.

[60] W. Caisheng, M. H. Nehrir, and S. R. Shaw, "Dynamic models and model validation for PEM fuel cells using electrical circuits," *IEEE Transactions on Energy Conversion,* vol. 20, pp. 442-451, 2005.

[61] K. Ou, W.-W. Yuan, M. Choi, S. Yang, and Y.-B. Kim, "Performance increase for an open-cathode PEM fuel cell with humidity and temperature control," *International Journal of Hydrogen Energy,* vol. 42, pp. 29852-29862, 2017.

[62] Y. X. Wang, F. F. Qin, K. Ou, and Y. B. Kim, "Temperature Control for a Polymer Electrolyte Membrane Fuel Cell by Using Fuzzy Rule," *IEEE Transactions on Energy Conversion,* vol. 31, pp. 667-675, 2016.

[63] M. W. Fowler, R. F. Mann, J. C. Amphlett, B. A. Peppley, and P. R. Roberge, "Incorporation of voltage degradation into a generalised steady state electrochemical model for a PEM fuel cell," *Journal of Power Sources,* vol. 106, pp. 274-283, 2002/04/01/ 2002.

[64] D. Zhang, "Contribution to prognostics of PEM fuel cells: approaches based on degradation information at multiple levels," Communauté Université Grenoble Alpes, 2018.

[65] R. Storn and K. Price, "Differential Evolution – A Simple and Efficient Heuristic for global Optimization over Continuous Spaces," *Journal of Global Optimization,* vol. 11, pp. 341-359, December 01 1997.

[66] D. Candusso, A. De Bernardinis, M.-C. Péra, F. Harel, X. François, D. Hissel, *et al.*, "Fuel cell operation under degraded working modes and study of diode by-pass circuit dedicated to multi-stack association," *Energy Conversion and Management,* vol. 49, pp. 880-895, 2008.

[67] A. De Bernardinis, M.-C. Péra, J. Garnier, D. Hissel, G. Coquery, and J.-M. Kauffmann, "Fuel cells multi-stack power architectures and experimental validation of 1kW parallel twin stack PEFC generator based on high frequency magnetic coupling dedicated to on board power unit," *Energy Conversion and Management,* vol. 49, pp. 2367-2383, 2008.

[68] B. Ozpineci, D. Zhong, L. M. Tolbert, D. J. Adams, and D. Collins, "Integrating multiple solid oxide fuel cell modules," in *Industrial Electronics Society, 2003. IECON '03. The 29th Annual Conference of the IEEE*, 2003, pp. 1568-1573 Vol.2.